Master's thesis

NTNU
Norwegian University of Science and Technology
Faculty of Natural Sciences
Department of Materials Science and Engineering

Magnus Bengt Inge Ramberg

Solid-solid Phase Change Material Pentaerythritol as a Latent Heat Storage Material in Domestic Cooking Stoves

Master's thesis in Materials Science and Engineering
Supervisor: Assoc. Prof. Julian Walker
Co-supervisor: Prof. Mari-Ann Einarsrud
June 2023

NTNU
Norwegian University of
Science and Technology

Magnus Bengt Inge Ramberg

Solid-solid Phase Change Material Pentaerythritol as a Latent Heat Storage Material in Domestic Cooking Stoves

Master's thesis in Materials Science and Engineering
Supervisor: Assoc. Prof. Julian Walker
Co-supervisor: Prof. Mari-Ann Einarsrud
June 2023

Norwegian University of Science and Technology
Faculty of Natural Sciences
Department of Materials Science and Engineering

NTNU
Norwegian University of
Science and Technology

Preface

This master's thesis is submitted as a part of the course *TMT4905 Materials Technology, Master's Thesis* in the spring semester of 2023 at the Norwegian University of Science and Technology (NTNU). The thesis is a continuation of the project work conducted in the course *TMT4500 Materials Technology, Specialization Project* [1] in the fall semester of 2022. Experimental work was performed by the author, Magnus Bengt Inge Ramberg, under the supervision of Assoc. Prof. Julian Walker, and Prof. Mari-Ann Einarsrud.

Acknowledgements

I would first like to express my deepest gratitude to my supervisor Julian Walker, for his invaluable guidance and support throughout the duration of this thesis. Your continuous encouragement, support, and inspiring attitude have been determining factors in the completion of this work, and for that, I am truly grateful. I would also like to thank my co-supervisor Mari-Ann Einarsrud for her guidance, and for making herself available throughout this thesis work. The lab engineers at the IMA labs, and the company Sunphase also deserve a big thanks. Without you, the completion of this thesis would not have been possible.

Last but not least, I want to send a heartfelt thank you to my family, my girlfriend, and my friends for your unwavering support through my studies. Your constant encouragement and belief in me have been a vital source of motivation and have played a pivotal role in my academic journey.

Abstract

The growing demand for energy consumption has brought thermal energy storage into the spotlight. Among its various approaches, latent heat storage stands out, where the heat is stored using the reversible phase transition of a phase change material. In this thesis, the mode of latent heat storage is discussed in the context of a thermal battery used to power a newly developed cooking stove. Throughout the study, material properties essential to latent heat storage are discussed, and the solid-solid phase change material and organic polyalcohol pentaerythritol ($C_5H_{12}O_4$) is considered as a potential candidate for the application.

Two experimental approaches were taken in order to form an understanding of the material's LHS properties. The first approach involved characterizing basic LHS properties such as specific heat capacity, thermal conductivity, and thermal expansion of the material. Here, differential scanning calorimetry, thermal diffusivity laserflash, and X-ray diffraction were utilized. The second experimental approach consisted of three paths investigating the thermal degradation of the material and the effect this had on the LHS properties.

The first two paths of the second experimental approach involved investigating how the atmospheric operating conditions and melting and resolidification process as well as the material's purity would affect thermal degradation, latent heat storage capacity, and the characteristics of the solid-solid phase change of the material. Differential scanning calorimetry, thermogravimetric analysis with mass spectrometry, and Raman spectroscopy were the experimental techniques chosen. The third and final experimental path studied how holding the material at the maximum operating temperature of $220°C$ for 7 days would affect the latent heat storage capacity and the characteristics of the solid-solid phase transition. The goal was to determine if the material properties were degrading. For the temperature hold experiment, it was made use of differential scanning calorimetry, Raman spectroscopy, and X-ray diffraction were utilized.

The findings from the investigations of pentaerythritol show a maximum enthalpy of change for the endothermic phase change of $311.56\ J/g$, with the phase transition starting at $184.51°C$. The specific heat capacity was determined to be between $1.43 - 2.06\ J/gK$ in the temperature range $40 - 160°C$. The thermal conductivity was determined to be between $0.93 - 0.56\ W/mK$ in the temperature range $25 - 175°C$. With XRD, the space group $I\bar{4}$, and linear thermal expansion coefficients $\alpha_a = 1.72 \cdot 10^{-5}$ and $\alpha_c = 15.39 \cdot 10^{-5}$ were found for the room temperature phase. The melting point of the material was determined to be $256.2°C$ in synthetic air, and $260.0°C$ in argon. Thermal cycling of the material showed that the highest purity material and an inert operating atmosphere are favorable for the highest heat capacity, and the least degradation. It was also observed that the material is highly susceptible to degradation during melting. Furthermore, an isothermal hold at $220°C$ for 7 days resulted in significant degradation of the material, indicating that the maximum temperature during operation is critical to the material's performance in LHS.

This study evaluated the influence of the operating atmosphere, maximum operating temperature, and purity on the latent heat storage properties of pentaerythritol. The findings identified that the atmosphere and maximum operating temperature as the two most critical factors affecting the lifetime and performance, with purity also playing a less significant role.

Sammendrag

Et økende energiforbruk har ført termisk energilagring i rampelyset. Blant ulike tilnærminger i termisk energilagring skiller latent varmelagring seg ut, der varmen lagres ved hjelp av en reversibel faseovergang i et fasovergangsmateriale. I denne oppgaven diskuteres latent varmelagring i sammenheng med et termisk batteri som brukes til å drive en nyutviklet kokeplate. Gjennom studien diskuteres materialeegenskaper som er essensielle for latent varmelagring, og det fast-fast faseovergangsmaterialet og organiske polyalkoholet pentaerytritol ($C_5H_{12}O_4$) vurderes som en potensiell kandidat for applikasjonen.

To eksperimentelle tilnærminger ble brukt for å danne en forståelse av materialets egenskaper innenfor latent varmelagring. Den første tilnærmingen involverte karakterisering av grunnleggende varmelagringsegenskaper som spesifikk varmekapasitet, termisk konduktivitet og termisk ekspansjon av materialet. Her ble teknikker som differensial sveip-kalorimetri, termisk diffusivitets laserflash og røntgendiffraksjon benyttet. Den andre eksperimentelle tilnærmingen besto av tre eksperimentelle veier som undersøkte termisk nedbrytning av materialet og effekten dette hadde på latent varmelagringsevne.

De to første veiene i den andre eksperimentelle tilnærmingen involverte undersøkelse av hvordan atmosfæriske forhold og smelte- og resolidifiseringsprosessen, samt materialets renhet påvirket termisk nedbrytning, latent varmelagringsevne og egenskapene til faseovergangsmaterialet. Eksperimentelle metoder som differensiell skanning kalorimetri, termogravimetrisk analyse med massespektrometri og Raman-spektroskopi ble benyttet. Den tredje og siste eksperimentelle veien undersøkte hvordan varmebehandling ved maksimal driftstemperatur på $220°C$ i 7 dager påvirket latent varmelagringsevne og egenskapene til faseovergangen. Målet var å bestemme om materialegenskapene ble svekket. For varmebehandlingseksperimentet ble differensial sveip-kalorimetri, Raman-spektroskopi og røntgendiffraksjon benyttet.

Resultatene fra undersøkelsene av pentaerytritol viste en maksimal endoterm faseovergangsentalpi på $311.56\ J/g$, der faseovergangen startet ved $184.51°C$. Spesifikk varmekapasitet ble bestemt til å være mellom $1.43 - 2.06\ J/gK$ i temperaturområdet $40 - 160°C$. Termisk konduktivitet ble bestemt til å være mellom $0.93 - 0.56\ W/mK$ i temperaturområdet $25 - 175°C$. Ved hjelp av røntgendiffraksjon ble romtemperaturfasen identifisert som romgruppen $I\bar{4}$, og lineære termiske ekspansjonskoeffisienter $\alpha_a = 1.72 \cdot 10^{-5}$ og $\alpha_c = 15.39 \cdot 10^{-5}$ ble funnet. Smeltepunktet for materialet ble bestemt til å være $256.2°C$ i syntetisk luft og $260.0°C$ i argon. Termisk sykling av materialet viste at høyere materialrenhet og en inert driftsatmosfære var gunstig for høyest varmelagringsevne og minst nedbrytning. Det ble også observert at materialet er svært sårbart for nedbrytning under smelting. Videre resulterte en isotermisk varmebehandling ved $220°C$ i 7 dager i betydelig nedbrytning av materialet, noe som indikerer at den maksimale temperaturen under drift er avgjørende for materialets ytelse i latent varmelagring.

Denne studien evaluerte innflytelsen av driftsatmosfære, maksimal driftstemperatur og renhet på latent varmelagringsegenskapene til pentaerytritol. Resultatene identifiserte atmosfæren og maksimal driftstemperatur som de to viktigste faktorene som påvirker levetiden og ytelsen, mens renhet spilte en mindre betydelig rolle.

Table of Contents

List of Figures

List of Tables

Acronyms

DSC Differential Scanning Calorimetry.

FTIR Fourier-transform Infrared Spectroscopy.

LHS Latent Heat Storage.

MS Mass Spectrometry.

PCM Phase Change Material.

PE Pentaerythritol.

SHS Sensible Heat Storage.

TCS Thermochemical Heat Storage.

TES Thermal Energy Storage.

TG Thermogravimetric analysis.

XRD X-ray Diffraction.

1 Background

1.1 Motivation

The discovery of fire is arguably one of the greatest gifts handed over to us by our ancestors. For them, this tool meant protection from dangerous wild animals, a source of warmth and lighting, and a way of constructing new tools and providing cooked food. Cooking played a central role in human civilization and evolution. The advent of new cooking technologies outperforming the campfire further increased the lives of humans to the point we are today. However, even today, not everyone has access to modern cooking technologies. According to World Health Organization, around 2.4 billion people worldwide continue to rely on less advanced cooking technologies, putting their health at risk due to indoor pollutants from these primitive technologies. It is estimated that an alarming 3.2 million premature annual deaths can be attributed to this systemic lack of modern technology [2].

These shocking numbers are a wake-up call to the world that the development of new, affordable, green, and safer solutions needs to be pushed. One specific way of approaching this problem lies in the realm of latent heat storage, a technology that currently is under rapid growth. Applying this technology in cooking stoves could prove to be a reliable, more affordable approach rather than going the route of energy storage in conventional batteries. It could increase energy efficiency, reduce non-renewable fuel consumption, and at the same time mitigate the risks of indoor air pollutants.

The way one could apply this material is by designing a cooking stove system around it and heating the material during the day with a heating element powered by solar cells. The heating element would make the material undergo its reversible endothermic phase change. When the sun sets, the heating of the material stops, and the phase change material would start to cool down, releasing a substantial amount of energy when undergoing the reversible exothermic phase change down to room temperature. A possible candidate for this specific use case is the solid-solid phase change material and organic polyalcohol pentaerythritol. The material has the potential for latent heat storage in cooking stoves due to its thermal properties, and the reversibility of its high enthalpy phase change. Determining factors like temperature range, heat storage capacity, and thermal stability all speak in favor of this candidate.

1.2 Aim

The aim of this master's thesis was to first investigate the research front of latent heat storage phase change materials with a focus on applicability in cooking stoves. Furthermore, the thesis aim was to examine the possibility of latent heat storage in the solid-solid phase change material and organic polyalcohol pentaerythritol. In order to achieve this two experimental approaches were shaped. The first aimed at investigating basic material properties essential for thermal energy storage (TES) such as specific heat capacity, thermal conductivity, and thermal expansion. This was made possible by utilizing differential scanning calorimetry (DSC), thermal diffusivity laserflash, and X-ray diffraction (XRD) analysis. The aim of the second experimental approach was to find out how atmospheric conditions, material purity, melting and resolidification of virgin material, and a temperature hold at the maximum operating temperature for an extended amount of time would affect the latent heat storage (LHS) properties of the material. Here, the operational temperature

range, phase change temperature, heat storage capacity, thermal degradation of the LHS properties due to thermal cycling of the material, and thermal degradation due to the maximum operating temperature were in focus. This was achieved by employing various experimental methodologies such as differential scanning calorimetry (DSC), thermogravimetric (TG) analysis with mass spectrometry (MS), Raman spectroscopy, and x-ray diffraction (XRD).

2 Introduction

This thesis explores the potential use of the organic polyalcohol pentaerythritol for thermal energy storage in cooking stoves. The following chapter provides a concise introduction to thermal energy storage, with a specific emphasis on latent heat storage. It also examines the essential parameters that need to be considered when choosing the right phase change material. Additionally, possible candidate materials for the stove application will be presented, and a thorough analysis of pentaerythritol will be carried out to determine its suitability for this purpose. By examining the material's properties, performance, and compatibility with cooking stoves, this research aims to establish whether pentaerythritol is a viable option for thermal energy storage in this application.

2.1 Thermal energy storage

Thermal energy storage (TES) systems aim to enable the storage of heat and cold within a TES medium for later release and utilization. This way of storing energy is not a new invention, on the contrary, the use of TES dates back to ancient times. Nowadays, one typically classifies TES into three main categories. Sensible heat storage (SHS), latent heat storage (LHS), and thermochemical heat storage (TCS), all with different applications. This thesis will focus on giving a comprehensive explanation of latent heat storage.

2.1.1 Latent heat storage

Latent heat storage (LHS) is the mode of storing thermal energy within the phase transition of a phase change material (PCM). This transition can occur when a material undergoes a phase change, encompassing solid-liquid, liquid-gas, solid-gas, or a solid-solid phase transition.

Comparing LHS with SHS and TCS, it is well known that the big advantages of LHS include a high energy storage density and a constant heat flow from the material during discharge. On the other hand, a major disadvantage when it comes to applying LHS in TES systems is that these materials often have low thermal conductivity. This means that the rate at which the heat is transferred is relatively low, and one would need to make an account for this in other ways depending on what material one is working with [3].

The way LHS works builds upon the mode of SHS, where the main factor that determines the amount of energy that can be stored and used is the specific heat capacity of the material (C_p). LHS takes another step by also including the energy used during a phase transition into the heat storage equation. This is referred to as the enthalpy of the phase change (ΔH). By combining the specific heat capacity and the enthalpy of change, one can determine the total amount of energy stored. Equation 2.1 presents this principle.

$$Q = \int_{T_i}^{T_{pc}} mc_{p,p1}dT + \Delta H_{pc} + \int_{T_{pc}}^{T_f} mc_{p,p2}dT \tag{2.1}$$

In equation 2.1, Q equals the total amount of heat stored, m is the mass of the LHS material, C_p is the specific heat capacity of the phase, dT is the change in temperature, and ΔH_{pc} is the enthalpy

of the phase change. Both C_p and ΔH_{pc} are dependent on the material.

Figure 2.1 illustrates this relationship between the temperature of the material and the amount of heat stored. Notice how the amount of heat stored increases significantly through the phase change of the material. This increase is attributable to the ΔH of the transition.

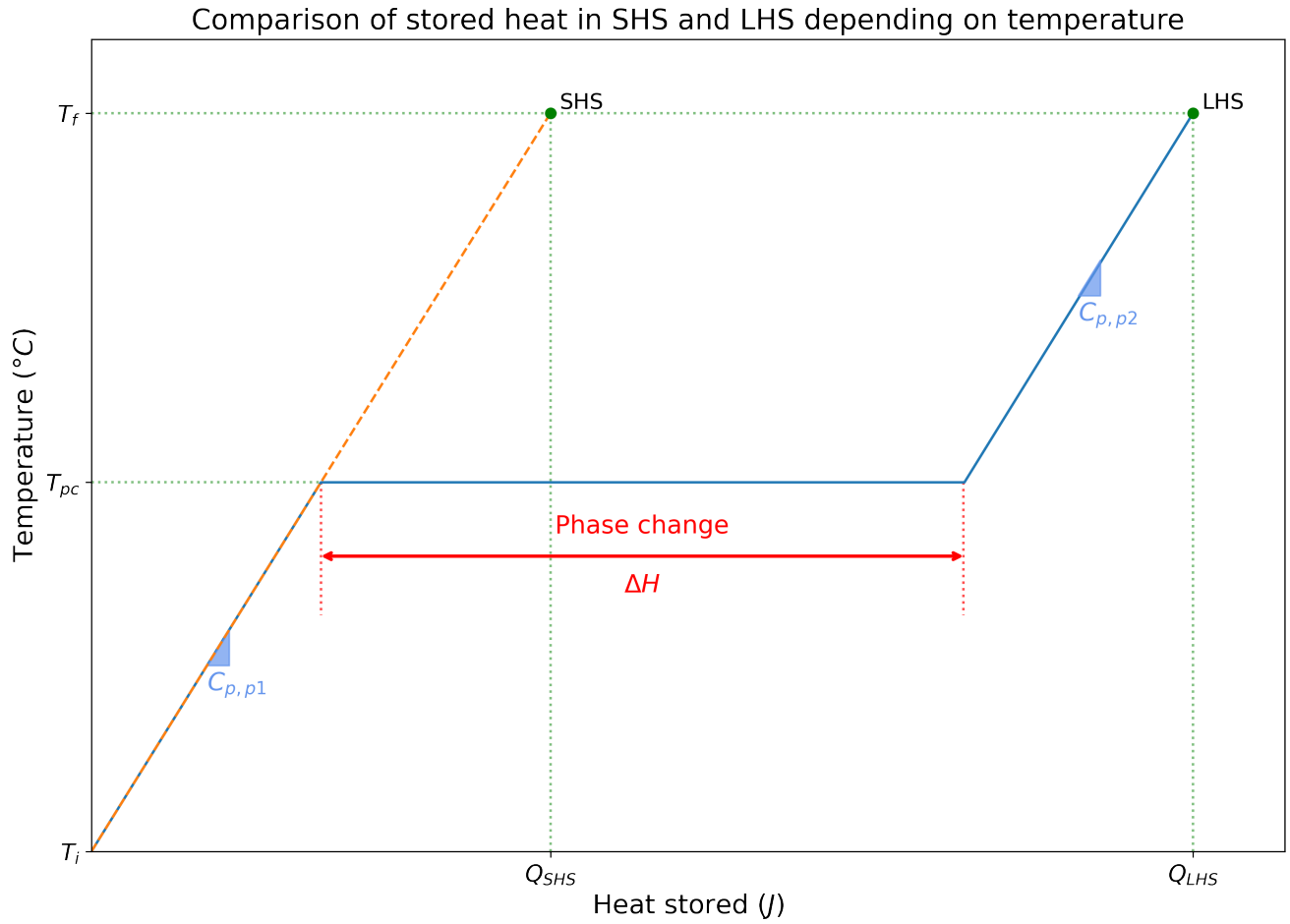

Figure 2.1: Visualization of equation 2.1. Comparing the relationship between SHS and LHS.

The solid-liquid phase transition is a commonly used phase transition in LHS. A big challenge of utilizing the solid-liquid phase change for LHS would be that the system has to be designed around dealing with a large volume change upon phase change. The liquid phase must be assessed carefully to avoid any leakage when melting the PCM. Macro-encapsulation of the solid-liquid PCM is a possible solution when talking about implementing these types of transitions. This has already attracted commercial manufacturers integrating the PCM into the building envelopes [4]. A frequently applied type of solid-liquid PCM used in LHS systems is paraffin waxes. These often have a low melting point, making them suitable for temperature control in buildings. Solid-gas and liquid-gas PCMs are often also complicated to implement in TES systems because of the massive volume change associated with the transition. An example of a liquid-gas TES system would be the gas-liquid heat exchanger. Upon discharge, the heat from the gas will be transferred over to the liquid whilst the gas undergoes a gas-to-liquid phase change.

Solid-solid PCMs used for TES are attractive because it solves problems the other types of phase

changes exhibit. The transition is one that involves a change in the crystal structure with little volume expansion compared to the other types of phase changes. This simplifies the implementation a lot, but there still is a need to consider the thermal expansion of the PCM in system designs. This minimal volume change during the solid-solid phase transition makes the solution leakage-free. This means that there would not be any need for encapsulation because of a flowing phase such as in solid-liquid TES systems. This thesis will take into consideration the solid-solid phase transition for TES purposes.

2.2 Applying phase change materials for latent heat storage

One typically classifies PCMs into three main categories. Organic, inorganic, and eutectic mixtures of the two. Organic PCMs include but are not limited to fatty acids, paraffins, and polyalcohols. Organic PCMs are often thought of as the ones with lower operational temperatures. However, studies on organic materials with higher phase change temperatures such as pentaglycerine, neopentylglycol, and pentaerythritol prove to hold some merit [5]. Inorganic PCMs are often metals and salt hydrates. The salt hydrates consist of a salt matrix bonded with water molecules. During the phase transformation upon charging, dehydration of the salt happens. The bonds holding the water molecules within the crystal structure break, and water molecules are released, leading to increased movement and temperature. Salt hydrates have a broad operating temperature range. As an example, studies on $CaO/Ca(OH)_2$ have shown promising results for TES in the temperature range of $400°C - 560°C$ [6]. The last main category is a combination of organic and inorganic materials. In the scope of this project, the organic PCM approach will be in focus, as a candidate material in this category seems to live up to the qualifications needed.

There have been plenty of studies conducted on organic PCMs of different purity suitable for LHS. Table 1 gives an overview of some important thermal properties of promising organic LHS PCMs. Here one can observe factors such as the phase change temperature of the transition used for heat storage, melting temperature, enthalpy of the phase change, thermal conductivity, and the material cost. All of these play a significant role in material selection. The following subchapter will explain important thermal properties to take into consideration when choosing the right material for heat storage in the cooking stove.

Table 1: LHS properties of selected organic phase change materials. The table lists the phase change temperature (T_{pc}), melting temperature (T_m), enthalpy of fusion (ΔH), thermal conductivity (k) liquid and solid (l,s), and cost of the material ($\$/kg$) from Sigma Aldrich and Fischer Scientific.

Material	$\boldsymbol{T_{pc}(^{\circ}C)}$	$\boldsymbol{T_m(^{\circ}C)}$	$\boldsymbol{\Delta H(J/g)}$	**k** $\boldsymbol{(W/mK)}$	**Cost** $\boldsymbol{(\$/kg)}$	**Ref.**
Solid-liquid						
D-mannitol	167	167	297	0.60	138	[7, 8, 9]
Erythritol	117	117	344	0.73	903	[10, 11, 12]
Xylitol	93	93	280	0.37s, 0.43l	113	[10, 13, 14]
Paraffin wax	64	64	173.6	0.35s, 0.17l	54	[10, 15, 16]
Glycerine	18.2	18.2	200.4	0.289	62	[5, 17, 18]
Solid-solid						
Pentaerythritol	187-189	255-259	290.3	0.106, 0.66-0.53	50	[19, 20, 21, 22, 23]
Tris	132	171.9	213.47	0.39	155	[24, 25, 26]
Pentaglycerine	82	200	166	0.232	75	[5, 27, 28]
Neopentylglycol	42-44	126	110.4-119.1	0.120	32	[5, 29, 30, 31]

2.3 Thermal capabilities

When selecting a material applicable for LHS, it is necessary to recognize the thermal properties which the material needs to exhibit to do its job. Among the most important factors that come into play are phase change temperature (and the melting temperature), the amount of energy stored within the phase change, the effective lifetime of the material (including the number of thermal cycles the material can go through, and the thermal degradation behavior), thermal diffusivity, and thermal expansion. It is also of interest to understand how the purity of the material can affect these properties.

2.3.1 Phase change temperature

Depending on the use of LHS material, it is important to choose one with a phase change temperature that lies within the useful temperature range of the application. As stated earlier, in the case of TES in a cooking stove, the transformation has to happen somewhere in the range of $80°C$ to $220°C$, preferably as high as possible. This narrows the search down considerably. As for possibilities within the solid-solid phase transition category, there are not many options available. From table 1, one can see that the materials pentaerythritol, tris (tris(hydroxymethyl)aminomethane), and pentaglycerine are the ones with the highest temperature of the endothermic solid-solid phase transition. Usually, polyalcohols and inorganic salt hydrates are good candidates for this temperature range.

One has to differentiate between the endothermic and the exothermic phase change, and consider both when applying a material for TES. It is recognized that numerous PCMs do not revert back to their initial phase solely upon reaching the phase change temperature. Instead, they begin transitioning back to their original state well after this temperature is reached. This phenomenon is called supercooling. In a TES scenario, a material with a large supercooling would not be able to store and release the heat of the phase transition at the same temperature range. Therefore it is important to consider both the endothermic (charging) phase change and the following exothermic (discharging) phase change [32]. Both need to lie within the desired operating temperature range.

Another factor that comes into play when talking about transformation temperature is the melting point of the material. If the purpose is to apply a PCM with a solid-solid phase transition, one wants to stay clear of any type of melting. Therefore it is beneficial if the phase transition utilized for heat storage and the melting transition lie far apart. In fact, it is best if any other transitions are as far away from the intended heat storage transition as possible. The reason for this is that when the material starts to undergo a phase transition that is not intended it may break the system as it is not designed for this purpose. Furthermore, the unwanted transition may result in material degradation, rendering the remaining PCM less effective, and maybe even unusable for TES.

Surface melting, also called premelting, is a phenomenon that needs to be mentioned when talking about transformation temperatures in PCMs. Surface melting occurs when the surface of a material melts while the bulk remains solid. This can have significant implications on the performance of the PCM as a LHS material. One can experience surface melting because of a sufficiently large temperature gradient in the material which lets the surface melt while the bulk remains solid at a lower temperature. The thermal conductivity of the material is one of the factors which influence this temperature gradient. A larger thermal conductivity would mean a more uniform temperature profile of the material and less likelihood of surface melting. Furthermore, the chance that the

material will experience surface melting increases as the surface energy of the material becomes substantially lower than that of the bulk. This could be the case for materials where there are a lot of intermolecular interactions within the bulk caused by for example Van-der-Waals forces and hydrogen bonds [33]. If a solid-solid PCM used for TES is subjected to surface melting, it has the potential to experience degradation. The liquid-solid transition of a solid-solid PCM is therefore not necessarily reversible.

2.3.2 Amount of energy stored in transition

When talking about a phase change material as a potential TES material, it is essential to question the amount of heat that can be stored and released when necessary. For application in a TES system, it is favorable that the amount of energy stored in a transition is as high as possible per volume and weight. This means the material has to have one or more reversible high entropy phase transitions where heat can be stored. As mentioned, LHS materials tend to have a high energy storage density. This is a property that makes them interesting for TES. Looking at table 1, one can see the materials erythritol and pentaerythritol are the ones with the highest enthalpy change going through the phase change used for heat storage. There are several chemical and crystallographic factors determining if a material has a high enthalpy of change. Both intermolecular and intramolecular bond strength plays a significant role, as breaking the bonds upon transition requires a certain amount of energy depending on the type of bonding. This makes it so that materials with a higher bonding strength generally have a higher enthalpy of change. In order to determine experimentally how high the enthalpy of change is, one can make use of differential scanning calorimetry (DSC). Here, the amount of thermal energy required to heat the material to a certain temperature, and undergo a phase transition is measured.

2.3.3 Effective lifetime

One of the most important factors after the operative temperature range and the amount of heat stored is the effective lifetime of the LHS material. When talking about effective lifetime, it refers to the number of times the material can undergo the thermal charging-discharging cycle without significantly degrading its TES properties to where it no longer serves its purpose. For a phase change material to be considered a good choice in a TES system, it has to have a sufficiently long effective lifetime. Depending on the application, an expected effective lifetime goal has to be set. In the case of the construction of the cooking stove, an effective 4000 thermal cycles with a degradation in enthalpy as low as 20% has been set as a requirement. Next to thermal cycling, the maximum operational temperature also plays a big role when talking about the effective lifetime. The economic viability is strongly affected by the effective lifetime of the storage medium, as a quicker degradation requires more frequent replacement, and therefore a higher material cost.

When talking about the effective lifetime, there are different angles of approach. One way to evaluate is by looking at how the material is affected by going through a repeated amount of thermal cycles over the phase change. Here, the phase change itself is in question. The answer that needs to be found is if the properties of the phase change are affected in a negative manner, such as a decreasing enthalpy of change (ΔH), or decreasing temperatures related to the transition such as starting temperature and end temperature. When the material goes through repeated phase changes, a number of things can happen. Bonds can potentially break, and new bonds may develop. Volume

change by changes in the atomic lattice can also occur. If the material cannot fully reversibly change back to the initial condition when discharging, its effective lifetime will become shorter, which can lead to reduced efficiency and increased cost for the TES system. To investigate if there are any amounts of degradation happening when cycling through the phase change, one could make use of apparatus such as differential scanning calorimetry (DSC). This analysis would determine if the enthalpy of change changes, and if the thermal characteristics of the phase transition (such as the start and end temperature of the phase change) are affected. Furthermore, X-ray diffraction (XRD) analysis could reveal changes in the material's crystal structure before and after cycling, and IR-spectroscopy will tell if the bonds of the material remain or if new bonds are developed.

Another approach one needs to consider when talking about the effective lifetime is the extended amount of time when the material is at its maximum operating temperature. When the material is heated to its maximum it may be prone to degradation. In this case, the charging phase transition itself may not be the problem, but rather the stability of the material when it is heated. As mentioned when talking about the phase change temperature, one wants to stay well clear of any other phase transitions that are not intended. If the material comes too close to this temperature, it may experience degradation caused by for example surface melting. An increased amount of time at this maximum temperature will also increase the chance that the material starts to degrade. Therefore, the temperature range and the temperature program needs to be carefully considered. Ways of investigating the potential for thermal degradation by a too-high operational temperature would be to test with thermogravimetric analysis (TG), and the previously mentioned methods to test for degradation when cycling through the phase change.

2.3.4 Thermal diffusivity

Thermal diffusivity within the LHS material is a very important aspect to consider as this may very well be the limiting constraint of the heat transfer in and out of the material. Thermal diffusivity is related to the thermal conductivity, density, and specific heat capacity of the material. This relationship is presented in equation 2.2, where α_{Tdiff} is the thermal diffusivity, k is the thermal conductivity, ρ is the density, and C_p is the specific heat capacity.

$$\alpha_{Tdiff} = \frac{k}{\rho C_p} \tag{2.2}$$

Recent studies have explored various approaches to address the low thermal diffusivity of organic PCMs. Here, the focus lies on finding applicable methods to help with heat transfer. One such study focuses on how to improve the problem of low thermal conductivity in paraffin used for LHS. This problem has been tackled in different ways. Absorbing paraffin (n-docosane) into expanded graphite (EG) is one such solution [34]. With a mass fraction of 10% EG, the thermal conductivity of the paraffin-EG composite was measured to be $0.82\,W/mK$, $0.60\,W/mK$ higher than for a mass fraction of 2% EG. This considerably decreased the melting time of the material, allowing for a more efficient storing of heat without lowering the melting point of the material. Another way of solving the problem of low thermal conductivity for solid-liquid LHS materials involves the use of finned pipes and metallic strips to lead the heat to and from the PCM [35]. There are many ways to solve the issues of heat transfer in PCMs, but the correct way is not necessarily the same for all materials and applications.

One way of measuring the thermal diffusivity is with a laserflash setup. Here, a laser pulse is sent through the sample material, and the time-dependent temperature rise is recorded. The thermal diffusivity, α_{Tdiff}, is calculated using the height of the sample, d, and the halftime, $t_{1/2}$ found where the temperature is half the maximum temperature of the sample. Equation 2.3 presents this relationship.

$$\alpha_{Tdiff} = 0.1338\frac{d^2}{t_{1/2}} \tag{2.3}$$

Using equation 2.2, and a modified equation 2.3, enables the calculation of the thermal conductivity from the laserflash measurements.

2.3.5 Thermal expansion

Thermal expansion is a phenomenon where a material's volume either increases or decreases due to a change in temperature. When a material is heated, the atoms start to vibrate. The movement of the atoms is what causes the material to expand. Depending on the type of material, one can have different degrees of thermal expansion upon heating and cooling. The thermal expansion coefficient is the determining material factor that says how much the material will expand with temperature. Equation 2.4 presents the linear thermal expansion. In this case, α_{exp} is the thermal expansion coefficient, ΔL is the total change in the length of the material, L_0 is the initial length of the material, and ΔT is the change in temperature over which the expansion or contraction has happened.

$$\alpha_{exp} = \frac{\Delta L}{L_0 \Delta T} \tag{2.4}$$

In TES applications with a LHS approach, it is important to consider the effects of thermal expansion for many reasons. The most obvious factor is that the structural integrity of the system can be damaged if the expansion is too great. An expanding material can lead to cracking or failure at places that are prone to high pressures. Furthermore, one has to consider the fact that when the material starts to shrink, one can experience leakage. This is because the material shrinks so much that gaps are formed between system components. In a LHS application, it is important to prevent leakage so that sufficiently high thermal conduction is maintained. Two ways one could investigate the thermal expansion of a LHS material are dilatometry and XRD. The first will measure the change in length of the material during heating, whilst the latter can discover the atomic positions at different temperatures and from that form a conclusion as to how the material expands or contracts.

2.3.6 Purity

When selecting a material for any application, the question of purity is one that is universal. For the case of LHS, it is essential to understand how the purity is related to the effectiveness of a specific PCM. One characteristic property that can be related to its purity is the melting point. It is known that one could estimate the material purity from the melting point of a material. As mentioned, in the case of LHS materials, the operational temperature range, and the temperature where the phase

change happens are two very important factors. A change in the melting point could potentially render the material useless for LHS. As an example, one could again take the LHS used in building envelopes [4]. If the purpose of using a PCM is to control the household temperature, a small shift in the phase change temperature could be detrimental for the TES system, as the operative temperature range for this specific application is very small (temperatures around $21°C$-$25°C$).

A less pure material may also be more prone to corrosion and degradation of the material in different ways. For example, the impurities may react with the LHS material over time, leading to the degradation of the material. These factors, and more, will impact the performance of the material in regard to heat storage. In the world of organic solid-solid phase change materials, a change in the crystal structure is what enables the storage of heat. If there are impurities present in the material this may change the way the transition commences, and one may end up with a crystal structure that is not favorable when it comes to the aspect of heat storage.

Impurities may also affect the thermal conductivity of the material. An impurity material with a lower thermal conductivity so that heat transfer will become slower. This may act as a bottleneck for the TES system making it less effective. On the other hand, as previously mentioned there have been conducted studies on how one can increase the thermal conductivity of LHS materials, and one solution would be to mix it with one with a higher thermal conductivity. This means that even though there is a chance that impurities can serve as a heat transfer hindrance for the system, it may very well also increase the thermal conductivity of the LHS material.

Purity is also especially important when it comes to the cost and availability of the material. It may be very difficult to obtain highly pure materials, and this will often come at a significantly higher price. This makes it so it is essential to carefully consider which purity is needed for the material to be the most effective in serving a role in a TES system.

2.4 Plastic crystals

A specific group of materials especially interesting when talking about LHS are plastic crystals. This group of materials is characterized by having a high-temperature mesophase, a plastic crystal phase, which is a phase that can be thought of as being somewhere between liquid and solid [36][37]. In this plastic crystal phase, the molecular structure of the material is still ordered on a global level, similar to what one can expect to find in a solid material. However, on a local scale, there is a structural disorder and rotational degree of freedom. This disorder is the origin of the high enthalpy of change that one can find in this phase transition.

In the eyes of LHS, plastic crystals fall under the solid-solid PCM category. There are several plastic crystal materials that have been investigated previously in a LHS context. Some of them can be found in table 1, including pentaerythritol, tris tris(hydroxymethyl)aminomethane), pentaglycerine, and neopentylglycol [25]. Among these, pentaerythritol has the highest enthalpy of change, and the highest operational temperature range. In light of these promising material parameters, the plastic crystal material pentaerythritol is further investigated.

2.5 Pentaerythriotol

Pentaerythritol (PE) is a commercially available material commonly used to synthesize several organic compounds such as explosives, plasticizers, and intumescent paints. Studies on the material give promising results for using PE as a LHS medium [20, 38, 39]. Throughout the rest of the thesis, the focus will lie on what makes this material so promising for TES, and if it lives up to the necessary requirements to be implemented for this purpose in a cooking stove.

PE is an organic material with a solid-solid phase transition that is characterized by a high enthalpy of change. Furthermore, the operational temperature range of the material seems to be sufficiently high to be used as a LHS material in cooking stoves up to $220°C$. Table 1 compares some of the material properties and the price for PE with other organic PCMs. The material classifies as a polyalcohol with the chemical formula $C_5O_4H_{12}$, where there is a central carbon atom and four arms of CH2-OH structures all held together with single covalent bonds. This allows the molecule to be flexible, and the branches can be rotated around the C-C or C-O bonds.

At room temperature, PE exhibits a body-centered tetragonal (BCT) crystal structure and is best described by the space group $I\bar{4}$ [40]. The intermolecular forces holding the molecules together on the (001) plane are hydrogen bonds. Furthermore, the layers of molecules are held together by the weaker van der Waals force on the crystallographic c-axis [41]. When heated, the material undergoes a solid-solid phase transition into a plastic crystal mesophase with a face-centered cubic (FCC) crystal structure. This happens at $187°C - 189°C$ [20]. At the phase transition temperature, the hydrogen bonds holding the molecules together break. The molecules themselves remain in place within the lattice because of the dispersion forces, but the breakage of these bonds introduces a higher degree of rotation so that the molecules can rotate more freely. This phenomenon, of a local disorder in the molecular structure whilst maintaining a globally ordered structure is often referred to as a plastic crystal phase. This mesophase is what makes TES with pentaerythritol so attractive.

The transition temperature of the material is specifically interesting. As mentioned, the endothermic solid-solid phase transition happens between $187°C - 189°C$. However, when cooling down from the plastic crystal phase, the material does not go through the phase transition before $169°C$ [20]. This means the material suffers from a degree of supercooling, but the exothermic reaction still happens at a reasonable temperature for a stove application.

When heating the material from room temperature, a specific amount of heat is required to increase the temperature by one degree. This is what is called the specific heat capacity. The specific heat capacity of high-purity pentaerythritol has previously been investigated. In between $60°C$ and $142°C$, a C_p of $1.55 - 1.99\ J/gK$ was reported for a 99.7% pure sample [42]. For higher temperatures above the solid-solid phase transition ($207°C$), it was reported values upwards of $2.77\ J/gK$. The specific heat capacity is the determining factor for sensible heat storage materials. As a comparison, water, which is a frequently used storage medium for SHS, is known to have a specific heat capacity of $4.1817\ J/gK$ at $25°C$ [43].

For LHS, however, the energy required to drive the phase change in question is the determining factor when it comes to the amount of energy stored. Equation 2.1 and figure 2.1 punctuate the importance of this phase transition for the TES system. This energy is referred to as the enthalpy of change (ΔH). Previous studies have been conducted to investigate how much energy goes into the phase transition of pentaerythritol. A study from 2019 reports a ΔH of $290.3\ J/g$ for the endothermic reaction, and $280.9\ J/g$ for the exothermic reaction of pentaerythritol with a purity of

98% [23]. Venkitaraj & Al. [41] reported seeing a ΔH of 264 J/g for charging, and 239 J/g for the solid-solid phase transition in 98% pure pentaerythritol. Other sources state values of ΔH upwards of 300 J/g for varying purity measurements [44, 45].

For pentaerythritol to be applicable in LHS, there is a need to investigate the amount of energy stored when one thermally cycles the material many times. It is necessary that the transition is reversible over a large number of cycles, meaning the enthalpy of change remains about the same. Through different studies, varying results have been reported. For PE of 98% purity, DSC results after 100 thermal cycles with a cycling program of $10°C/min$ heating/cooling up/down to $210°C/30°C$ showed that the enthalpy of the transition had decreased 6.8% upon charging and that the transition temperatures had remained stable [20]. This study was conducted under uncontrolled atmospheric conditions. Another study conducted on a pentaerythritol-0.0625 $wt\%$ copper sample showed an 8.82% reduction in enthalpy upon charging after 1000 thermal cycles [23]. These studies seem to correspond fairly well, and there is reason to believe that pentaerythritol has the potential to be applied in TES.

The thermal conductivity of PE is relatively high compared to other organic PCMs. A previous experimental study reported that pure 98% PE had a thermal conductivity of 0.106 W/mk [20]. Here, the density was measured using the Archimedes principle, and the thermal diffusivity was found with laserflash. Another experiment where the thermal conductivity was found by melting and casting the material before measuring the thermal conductivity with the TPS technique. Values between 0.66 W/mK and 0.53 W/mK in the temperature range $30 - 180°C$ [22]. As previously mentioned, organic PCMs are known to have relatively bad thermal conductivity. This, however, could be mitigated by mixing with other elements that have a higher thermal conductivity. In the same study that found the thermal conductivity of pure 98% PE [20], they also had samples containing up to 0.5% indium of 99% purity in powder form. It was shown that these samples had a higher thermal conductivity and that the downward trend in thermal conductivity with temperature as seen previously was the same for these samples.

Before the solid-solid phase transition is reached, the material undergoes volume change due to increasing movement in the atomic lattice. This volume change can be measured quantitively as the thermal expansion coefficient. Because the material has a BCT structure in the low-energy phase, two thermal expansion parameters can be found. Chandra et al. measured the thermal expansion in the a, and c directions to be $\alpha_a = 2.6 \cdot 10^{-5}, \alpha_c = 14 \cdot 10^{-5}$ [46]. The fact that the c-parameter seems to be so much larger originates in the previously mentioned theory of what bonds can be found in the molecule. On the c-axis the lower energy Van-der-Waals bonds are holding the molecules together, whilst the slightly higher energy hydrogen bonds work in the (001) plane.

The most common impurities in commercially available pentaerythritol are di-pentaerythritol, a formal of unestablished structure, and formaldehyde. Formaldehyde plays a key role in the resolidification of the material after melting. It has been shown that the presence of formaldehyde reduces the growth rate of pentaerythritol crystals. Di-pentaerythritol and the formal did not appear to affect recrystallization [47].

2.5.1 Degradation of penterythritol

A central subject when talking about implementing a PCM for LHS is degradation. If the material starts to degrade upon heating, it may very well be impossible to utilize it for its intended application.

For PE it is therefore necessary to establish how the material degrades so that one could reflect upon whether it is a suitable candidate for LHS in the beforementioned cooking stove application.

A study on the thermal decomposition of PE in an intumescent coating context looked at how the material changes upon heating depending on the atmosphere, nitrogen, or air [48]. The experimental procedures involved TG and Fourier transform infrared spectroscopy (FTIR). The TG experiment demonstrated that the 5% weight loss occurred at $223°C$ in an air atmosphere and at $235°C$ in nitrogen. The maximum loss of material was seen in air and nitrogen atmospheres at $270°C$ and $288°C$, respectively. It was concluded that oxygen promotes the thermal decomposition of the material. The Raman results further confirmed this by seeing larger amounts of $-OH$ being produced when the material was heated in air.

A similar study of the material proposed that this production of $-OH$ was in fact a dehydration reaction taking place during the heating of the material. Here, H^+ is removed, and together with the oxygen in the atmosphere H_2O is created. Two ways of decomposition were proposed to be likely [49]. This proposition can be seen in figure 2.2.

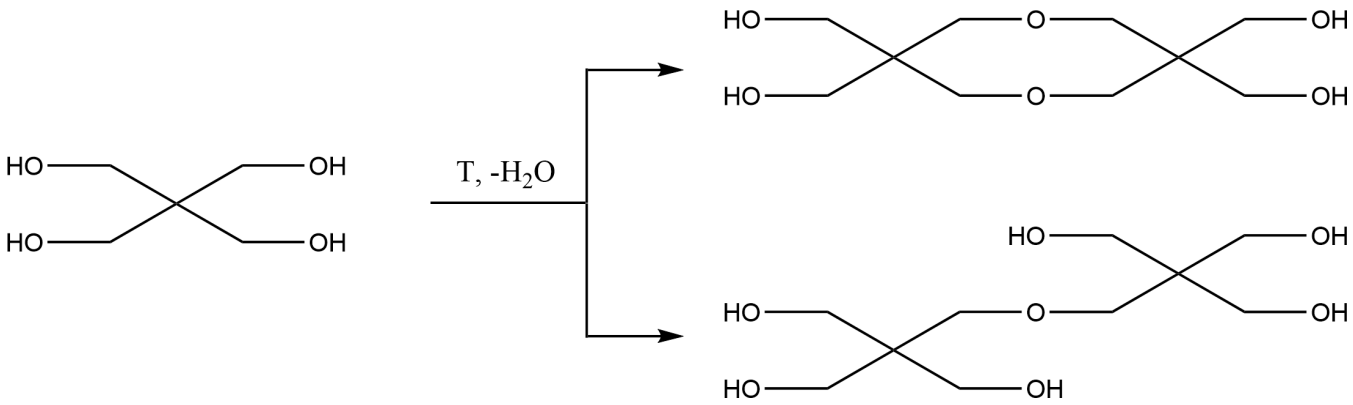

Figure 2.2: Decomposition of pentaerythritol. Creation of [3,7,7-tris(hydroxymethyl)-1,5-dioxocan-3-yl]methanol (top), and dipentaerythritol (bottom). H_2O is created when hydrogen is removed from the molecule and reacts with oxygen in the atmosphere.

A third study researching the decomposition of pentaerythritol upon heating in intumescent paints in an acidic environment proposes that the material decomposes into formaldehyde and acetaldehyde [50]. This decomposition is illustrated in figure 2.3.

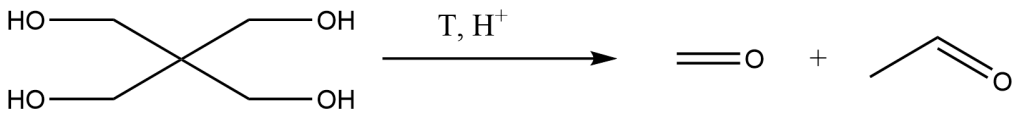

Figure 2.3: Decomposition of pentaerythritol. Creation of formaldehyde and acetaldehyde in an acidic environment.

Evidently, there are several paths of decomposition when it comes to the degradation of the material. Knowing what bonds are broken, and in which order is not trivial. Looking at the energy of

formation of the bonds displayed in table A.1, one can see what the bond energies for the single bonds found in the pentaerythritol are. These bond energies are the amount of energy needed to break that specific bond. Ideally, using this table one could say that the bonds with the lowest energy break first upon heating. However, this is not the case as intermolecular forces also affect how the decomposition of the molecule will happen. As an example, one could look at a study on the decomposition of ethanol [51]. Here, it was found that at different temperature and pressure conditions, different ways of decomposition were dominating. Below 10 atm, the decomposition from ethanol to $C_2H_4 + H_2O$ was found to be dominating, and at higher pressure over $1500K$, the decomposition from ethanol to $CH_3 + CH_2OH$ was the dominating reaction. This proves that one could not make a conclusion as to what bonds break first based solely on the bond energies.

3 Experimental

To investigate the applicability of pentaerythritol as a TES medium, several experimental investigations were conducted. Figure 3.1 illustrates how the project was approached from an experimental angle.

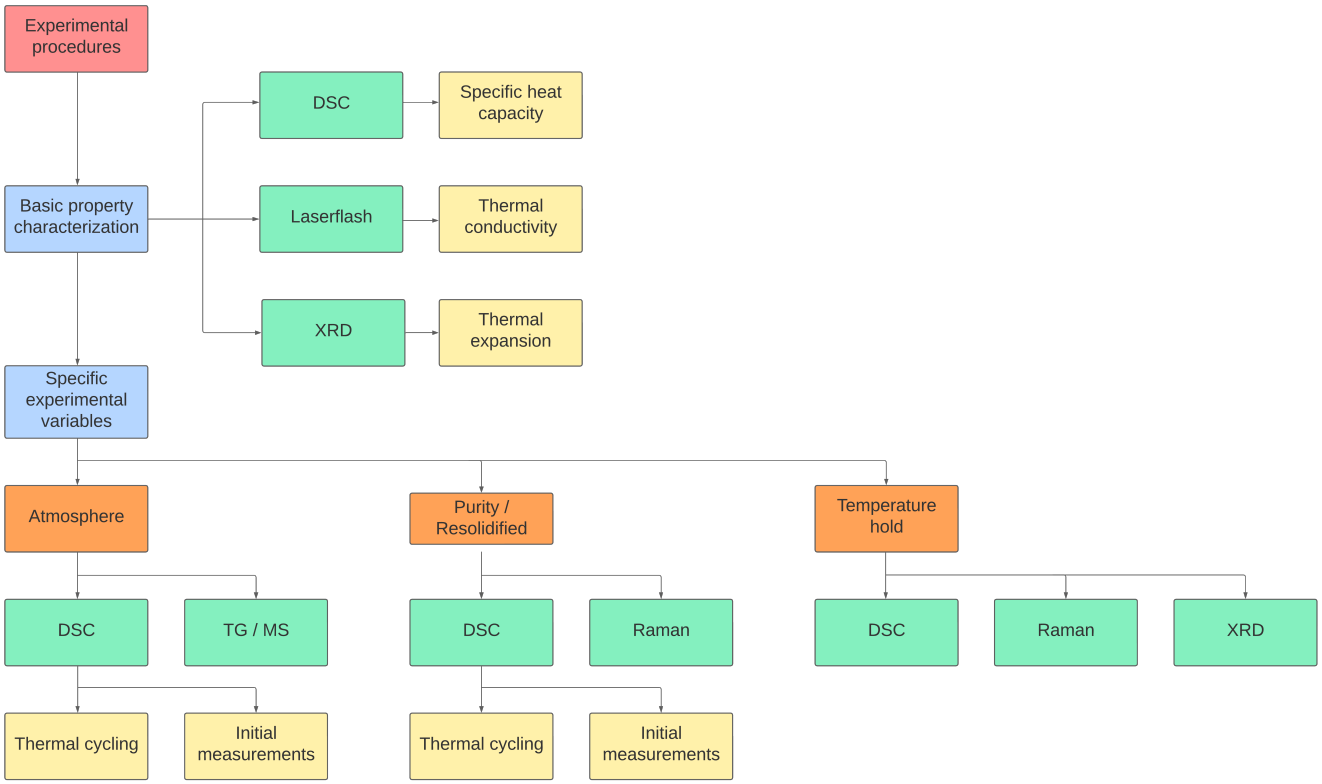

Figure 3.1: Experimental plan. A set of basic property investigations and three experimental paths to investigate how varying specific variables affects the material's TES properties.

As shown in figure 3.1, the project has been divided into one initial investigation of basic property characterization, and a three-part investigation of how the material's LHS properties were affected by changing some experimental variables. The initial investigation aimed at investigating the properties of specific heat capacity, thermal conductivity, and thermal expansion. This was done using DSC, laserflash, and an XRD apparatus. The first of the three-part investigation aimed to investigate how the material's TES properties were affected by the operational atmosphere. Here, the comparison between an argon working atmosphere and a synthetic air atmosphere was made. The second part aimed to establish if the material's TES properties were significantly diminished by lowering the purity of the material, or melting and resolidifying the material. Lastly, the third part investigated how the material properties were affected by holding the material at the maximum operational temperature for an extended amount of time.

Throughout all the investigations apparatus known to be able to investigate the relevant properties of LHS materials were utilized. This includes differential scanning calorimetry (DSC), laserflash, X-ray diffraction (XRD), thermogravimetric analysis with mass spectrometry (TG with MS), and Raman spectroscopy. This chapter will present the experimental programs seen in figure 3.1.

3.1 Material and initial sample preparation

The materials that were investigated were supplied by two different suppliers. Two pentaerythritol purities, 99 $wt\%$ and 86 $wt\%$ of pentaerythritol from Perstorp (P98 & P86), and two purities, 99 $wt\%$ and 98 $wt\%$ from Sigma-Aldrich (SA99 & SA98). All of the samples were delivered in powder form. Every powder was ground down with a pestle and mortar into fine powders so that the particle size difference was similar. A melted material sample (MP98) was also made from the P98 sample. This was done using a hot plate, heating the P98 material in a boron-silicon glass beaker with a thermocouple attached to monitor the temperature. After the material was fully liquid, it was poured onto a bent sheet of aluminium paper and cooled down at room temperature. This was all done within a fume cupboard with an uncontrolled atmosphere. After the solidification, the melted material also was ground down with mortar and pestle into fine powder.

3.2 DSC

Differential scanning calorimetry (DSC) was used as a tool to find the specific heat capacity, enthalpy of transition, and characterize the important temperature markers for the solid-solid phase change. Furthermore, the DSC investigations involved thermally cycling samples of PE at different atmospheric conditions whilst measuring the amount of thermal energy going into and out of the samples. All the samples, (P98, P86, MP98, SA99, and SA98) were subjected to this procedure. The instrument used was a Netzsch DSC 214 Polyma with aluminium crucibles.

3.2.1 Specific heat capacity

The intention of the first DSC program was to find the specific heat capacity of the P98 material before the solid-solid phase transition. To achieve this, a temperature program was first created where two thermal cycles from 25°C to 220°C were planned. The heating and cooling rate was 10°C/min, which was made possible by using liquid nitrogen in the nitrogen gas flow. When reaching the maximum and minimum temperatures, the temperature was held isothermally for five minutes. Furthermore, the measurement was conducted in synthetic air with a flow of 20 ml/min, and a nitrogen gas flow of 40 ml/min. Nitrogen was also used as a protective gas with a flow of 60 ml/min. A small sample size of around 10 mg was measured out, and the sample was put inside a pierced-lid aluminium crucible. Figure 3.2 presents the temperature program for the specific heat capacity measurement.

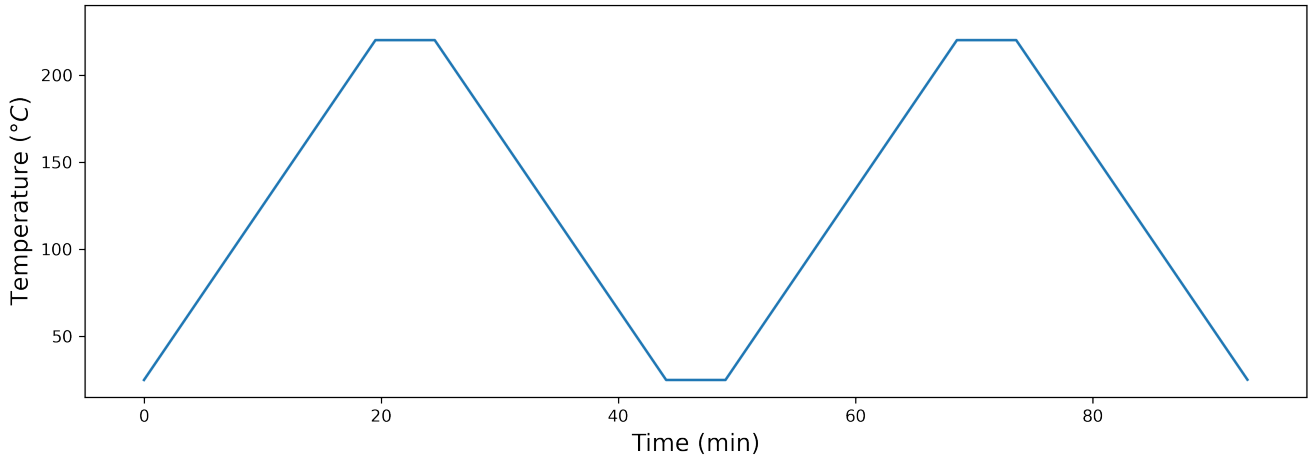

Figure 3.2: DSC temperature program for the C_p measurements. Starting temperature of $25°C$, a maximum temperature of $220°C$, and holding times of 5 minutes at the end of heating and after the first cooling. Heating/cooling rate of $10°C/min$.

In order to find the specific heat capacity of the material, a reference run had to be conducted. Here, a sapphire reference with a known C_p was used. After the reference was run, the PE sample itself went through the same temperature program. In the analysis software Protheus (by Netzsch), the C_p-ratio method was used to find the specific heat capacity of the material.

3.2.2 Initial phase change measurements

The initial DSC measurements for varying atmospheric and purity conditions aimed to give an understanding of the enthalpy of transition and key temperatures of the transition for all of the virgin material samples. Furthermore, sample MP98 was also tested this way. Here, two-cycle runs were conducted. The temperature ranged from $25°C$ to $220°C$, with an isothermal hold for $5\,min$ before cooling down to $100°C$ and a thermal hold of another $5\,min$. Then the samples were heated back up to $220°C$ before an isothermal hold for another $5\,min$. Lastly, the samples were cooled back down to $25°C$. The heating and cooling rate throughout the whole process was $10°C/min$, which was made able by liquid nitrogen cooling through the nitrogen gas flow. The temperature program for the initial DSC mapping of the samples can be seen in figure 3.3. The measurements were conducted in both a synthetic air atmosphere and an argon gas atmosphere. The gas flows were $20\,ml/min$ of synthetic air/argon gas in the oven, $40\,ml/min$ of nitrogen gas, and $60\,ml/min$ of protective nitrogen gas for all temperature programs.

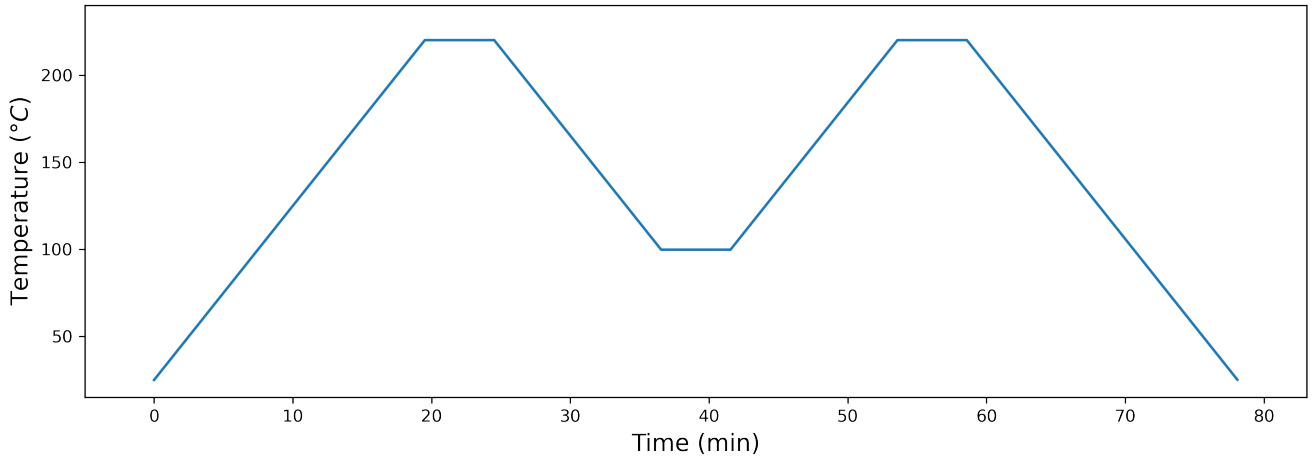

Figure 3.3: DSC temperature program for the initial DSC measurements. Starting temperature of $25°C$, a maximum temperature of $220°C$, a cooling down to $100°C$, and holding times of 5 minutes at the end of heating and after the first cooling. Heating/cooling rate of $10°C/min$.

3.2.3 Thermal cycling measurements

The thermal cycling measurements with DSC consisted of 10 consecutive thermal cycles, taking 8 hours in total. This program was designed with the intent of investigating the reversibility of the phase change and degradation upon repeated thermal cycling of the material. Sample P98, P86, MP98, SA99, and SA98 were all subjected 50 cycles each in both a synthetic air and argon atmosphere. During these measurements, liquid nitrogen was not applied due to problems with the instrument. The heating rate was set to $10°C$, whilst the cooling rate was set to $5°C$ because of the lack of liquid nitrogen. The temperature program ranged from $25°C$ to $220°C$, and down to $100°C$ between each cycle. After each dynamic step except for at the end, an isothermal hold was conducted for $5\,min$. Figure 3.4 illustrates the temperature program that was followed for the thermal cycling in DSC. The gas flows for the thermal cycling measurement were the same as for the initial DSC investigation.

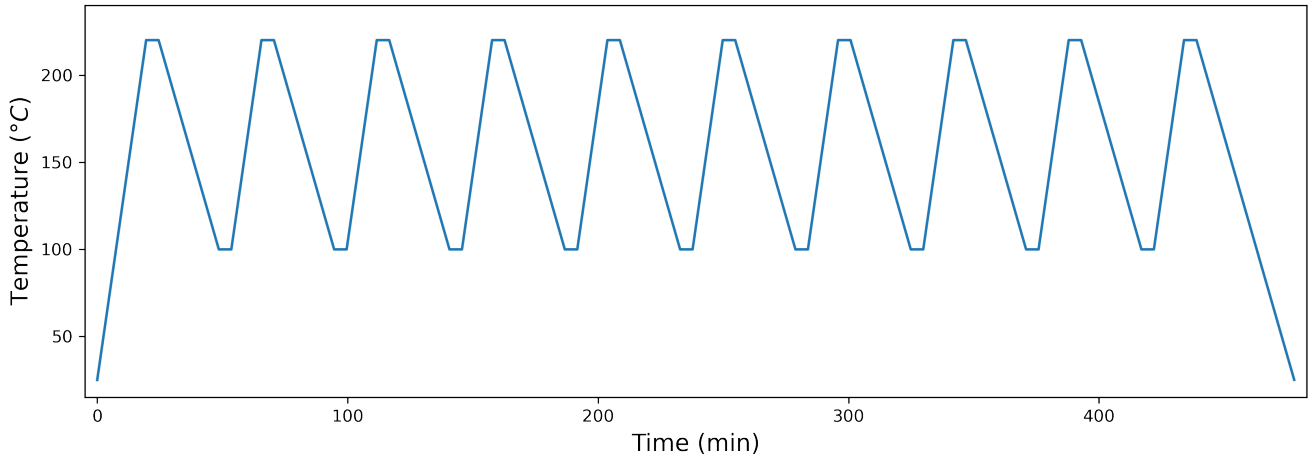

Figure 3.4: Temperature program for the thermal cycling DSC measurements. Following the same temperature program as seen in figure 3.3, but cooling rate of $5°C/min$, and 10 cycles instead of 2.

3.2.4 Temperature hold measurements

As a complementing experiment to the thermal cycling in the DSC, a thermal hold experiment was conducted where a melted and re-solidified sample of P98 was investigated by holding the material at $220°C$ in an oven for 7 days. The material was melted in a similar manner to the sample MP98, and when liquid, it was poured into an alumina crucible and cooled down at room temperature.

A calcination oven was prepared at $220°C$ in a fume hood. Before placing the re-solidified sample in the oven, the temperature in the area where the crucible was to be placed was controlled with two external s-type thermocouples. After the oven temperature stabilized with a program set to $220°C$, the temperatures measured were $10\,cm$ apart, $231.1°C$ in the air right above the center, and $235.6°C$ at the bottom center where the crucible was to be put. An average between the two would therefore be $233.35°C$, $13.35°C$ higher than the wanted temperature. Figure 3.5 illustrates how the real temperature was found, and how the sample crucible was placed inside the oven during the temperature hold.

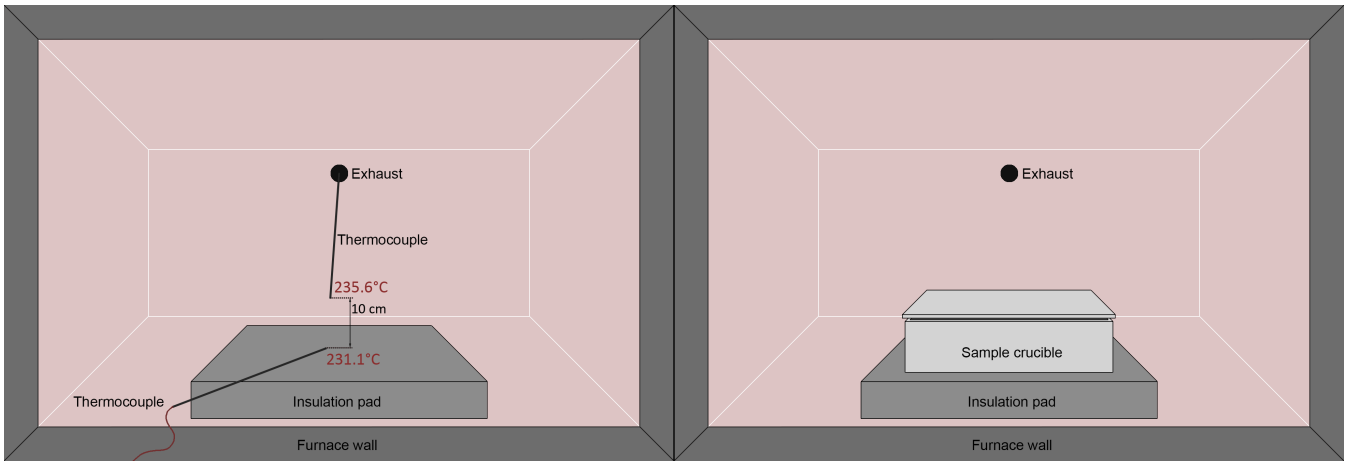

Figure 3.5: Illustration of calcination oven temperature calibration and crucible placement. Placement of thermocouples on the left in temperature calibration, and placement of sample crucible on the right during temperature hold.

Taking this into consideration, a temperature program of 207°C was chosen to make sure the real temperature was closer to 220°C in the local area where the sample was to be placed. The oven was preheated for two hours before placing the alumina crucible with the P98 sample inside, making sure the temperature had stabilized. The sample was left in the oven for one week. Every 24 hours, the sample was briefly taken out, and a small part of the surface of the sample material was taken out to be analyzed with DSC. After the sample had been in the oven for 7 days, it was taken out, and a part of the sample was also taken out to be analyzed with XRD and Raman spectroscopy. The XRD and Raman procedures will be discussed later in this chapter.

The DSC program used to investigate the samples is the same as the initial phase change measurements in section 3.2.2, and the temperature program can be seen in figure 3.3, with the exception that the cooling rate was turned down to 5°C/min due to the lack of liquid nitrogen.

3.3 TG with MS

To investigate the thermal degradation of pentaerythritol over the entire operating temperature range, two measurements were conducted in TG (Netzsch - STA449 C Jupiter) connected to MS (Netzsch - QMS403 C). The first measurement was conducted in a synthetic air atmosphere, and the second in an argon atmosphere. The temperature program that was followed was a 5-minute isothermal hold at 40°C, a heating to 500°C with a heating rate of 10°C/min, an isothermal hold for 10 minutes, and lastly a cooling down to 40°C with a cooling rate of 10°C/min. Figure 3.6 illustrates this thermal program. The entire temperature segment used the purge gas synthetic air or argon with a flow of 20 ml/min, and the protective nitrogen gas with a flow of 20 ml/min. For both measurements, a background was first measured, which was later subtracted in the analysis. Regarding the MS, all molecular weights up to 100 g/mol using a bar graph scan.

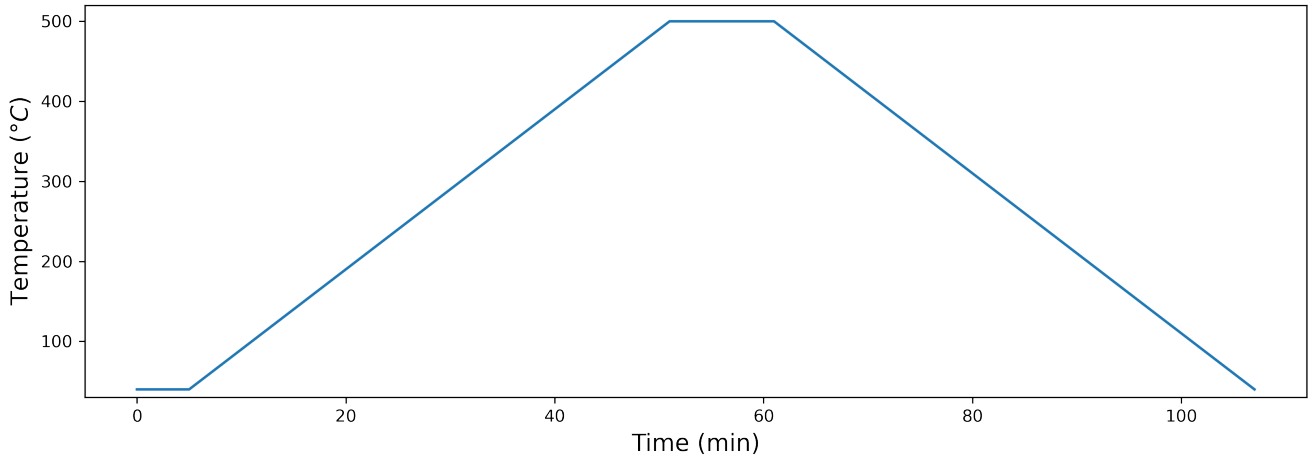

Figure 3.6: TG with MS temperature program. Initial temperature hold at 40°C before increasing the temperature to 500°C at 10°C/min. Hold for 10 minutes at maximum temperature before cooling back down with a cooling rate of 10°C.

3.3.1 Laserflash

In order to try to measure the thermal diffusivity of melted and resolidified material, a batch of melted P98 material was cast into pellets with an initial diameter of 15 mm and a small varying height. When the material had solidified and cooled down, the pellets were taken to a polishing station where the height of the pellet was ground down to 2.11 mm, and the diameter ground down to an average of 12.08 mm. This was done by utilizing SiC grinding papers of varying sizes. The weight of the pellet was measured at 0.2915 g. The bulk density of the pellet was calculated to 1.205 g/cm^3 using the dimensions measured with a caliper and a lab scale. After the pellet shaping was completed, a layer of graphite was sprayed onto the entire surface so that the sample could be tested. An ideal case of laserflash in the utilized apparatus on a PE pellet would have a height as small as possible, preferably less than 1 mm, and a diameter of 12.5 mm.

The apparatus utilized for the laserflash measurements was a Netzsch - LFA 457 MicroFlash, and the measurement was run in air. The experiment was conducted at varying temperatures; 25°C, 100°C, 150°C, 175°C, and 200°C. The heating rate between the temperature steps was 5 K/min, and for the last step 10 K/min. For each step, there was an isothermal hold of 5 min before the measurement started. For each temperature step, 5 measurements were conducted, and an average result and standard deviation were calculated.

3.4 XRD

3.4.1 Thermal expansion investigation

To determine the thermal expansion of the material upon heating, X-ray diffraction (XRD) was utilized with a heating element on a sample of SA99. The instrument used to conduct measurements was a Bruker AXS D8 Advance, and the software used to analyze the results was Bruker

DIFFRAC.EVA, and DIFFRAC.TOPAS. The temperatures programmed for investigation were $30°C$, $60°C$, $85°C$, $110°C$, $135°C$, $160°C$, $185°C$, $210°C$, $235°C$, and $260°C$. Other instrumental configurations included a $k\alpha$ source of Cu with a wavelength of 1.5406Å, a 2θ range from 15° to 70°, fixed divergence slit of 0.5°, step size of 0.025°, and a temperature holding time of 5 minutes before each measurement.

Before conducting the measurements, a temperature calibration had been run on a sample of alumina. Here temperatures up to $1000°C$ had been investigated. It was estimated that between $100 - 200°C$, the offset was $15.5°C$ above the programmed temperature. After the measurement was conducted, the results were analyzed using the beforementioned software, and the lattice parameters were found with Pawley-fitting to the space group $I\bar{4}$ for every temperature.

3.4.2 Temperature hold measurements

Two XRD measurements were conducted on samples from day 0, and day 7 of the temperature hold experiment. The instrument used to conduct these two measurements was a Bruker D8 Focus, and the software used to analyze the results was the same as for the previous XRD experiment described in section 3.4.1. The XRD scan was done at room temperature. Here, a divergence slit of $0.2\,mm$ was utilized. A 2θ range from 15° to 90° was investigated, and a k_α source of Cu with a wavelength of 1.5406Åwas used. After the measurements were completed, the results were analyzed with the beforementioned software, and the peaks were located and indexed in order to observe any difference between the two measurements.

3.4.3 Raman

Raman measurements were conducted on fresh P98 material in room temperature conditions and on material from day 0 and day 7 in the isothermal hold experiment. The apparatus used was a WITec Alpha 300R, and the measurement configuration included an integration time of 10 seconds, 20 accumulations, and a laser emission wavelength of $532\,nm/5.0\,eV$. The measurements were performed with a $50X$ microscope objective with a $1\,mm$ working distance.

4 Results

4.1 DSC

4.1.1 Specific heat capacity

The first of the basic property characterization measurements were the DSC measurements of the specific heat capacity. The result from this measurement can be seen in figure 4.1. Here, one can see an increasing specific heat capacity leading up to the endothermic phase change. At $40°C$, the P98 sample had a specific heat of $1.43\ J/gK$. This value had increased to $2.06\ J/gK$ at $160°C$.

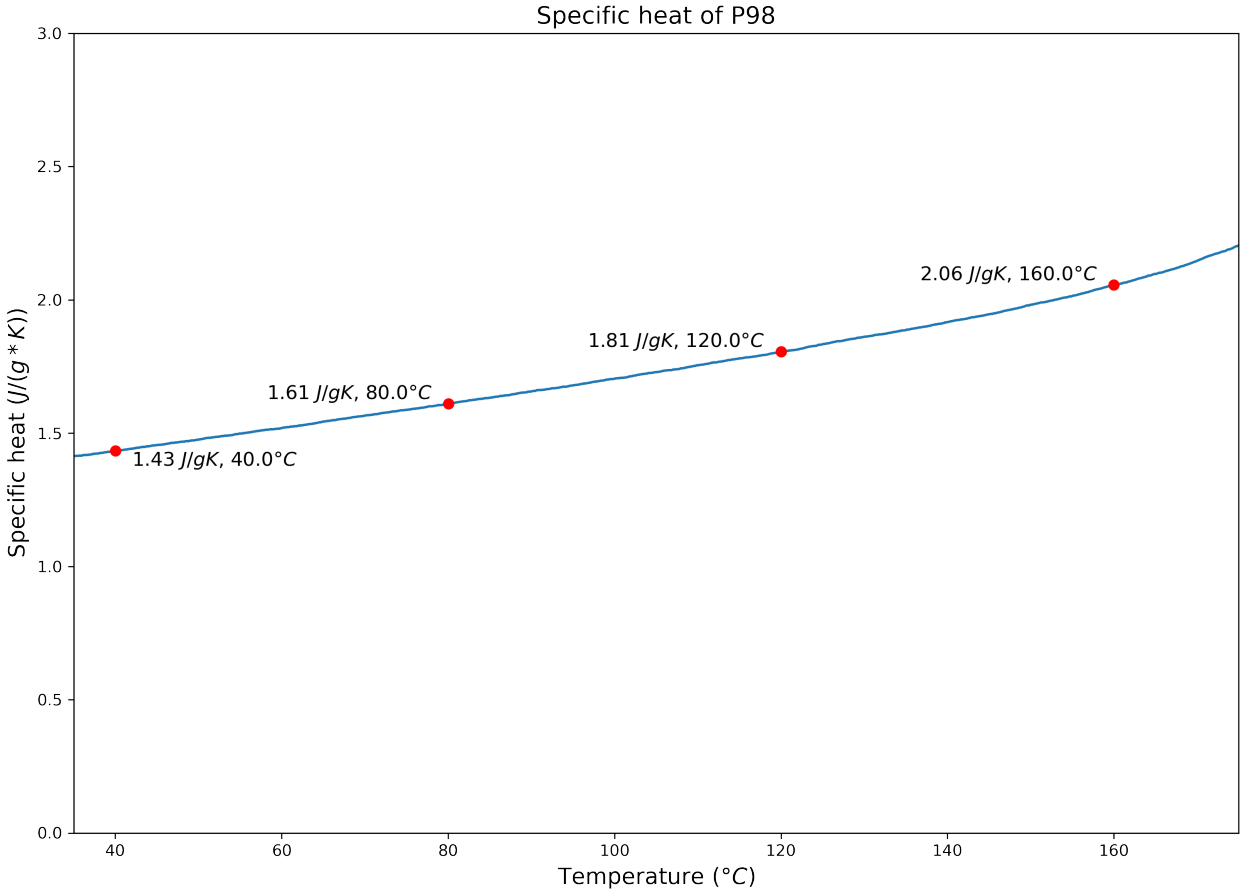

Figure 4.1: Measured specific heat capacity in the temperature range below the solid-solid phase change. Data was gathered with DSC C_p-ratio method.

4.1.2 Initial phase change measurements

The initial investigation of the material's TES properties such as the total amount of energy stored in the endothermic phase transition, and other characteristics of the phase transition itself were investigated through the experimental procedures described in section 3.2. The results from the experimental DSC procedure described in section 3.2.2 are presented in figure 4.2 and figure 4.3.

Here, the heat flow in the measurement is plotted against the temperature in the oven. For all the initial DSC measurements two cycles were conducted, and the second cycle was the one plotted and analyzed.

The first figure is of the sample P98 in a synthetic air atmosphere. Here, one can observe how the enthalpy of the transition is found. The start and endpoint of the transition were determined using a mathematical function, and the area under the peak was found by integrating the heat flow curve depending on time. Other values such as the FWHM, and the temperature at the bulk transition (the peak) were also found in order to be able to say more about the characteristics of the endothermic solid-solid transition. As one can see, the material is first heated from $100°C$ up to approximately $184.5°C$. Then, the heat flow suddenly becomes large before reaching a maximum at approximately $197.2°C$. From there, the heat flow into the material becomes smaller, and the baseline of the heating is reached when the temperature approaches approximately $213.6°C$. The material is further heated to $220°C$, where it is held for five minutes. After this isothermal step, the material is cooled back down to room temperature. One can observe this cooling by seeing that the heat flow is in the negatives, meaning there is a heat flow coming out of the sample. At approximately $172.2°C$, there is a substantial exothermic release of energy. This release peaks at $167.4°C$, and goes back to the exothermic baseline when the temperature reaches approximately $157.8°C$. From there, there are no further exothermic peaks. It is also worth noting the points where there is a heating/cooling rate change from the isothermal steps. This is right after $100°C$ in the endothermic area, and right after the isothermal step when starting to cool down the material from $220°C$ in the exothermic area. This change in heating/cooling rate creates artifacts in all of the DSC plots shown as small peaks in the endothermic and exothermic areas.

The errors in the measurements were found by running five 2-cycle DSC measurements of five different P98 samples. These results were analyzed, and the standard deviation in enthalpy of the exothermic phase change was found to be $\pm 0.88\, J/g$, whilst the error in the temperatures associated with the phase change was found to be $\pm 0.74°C$.

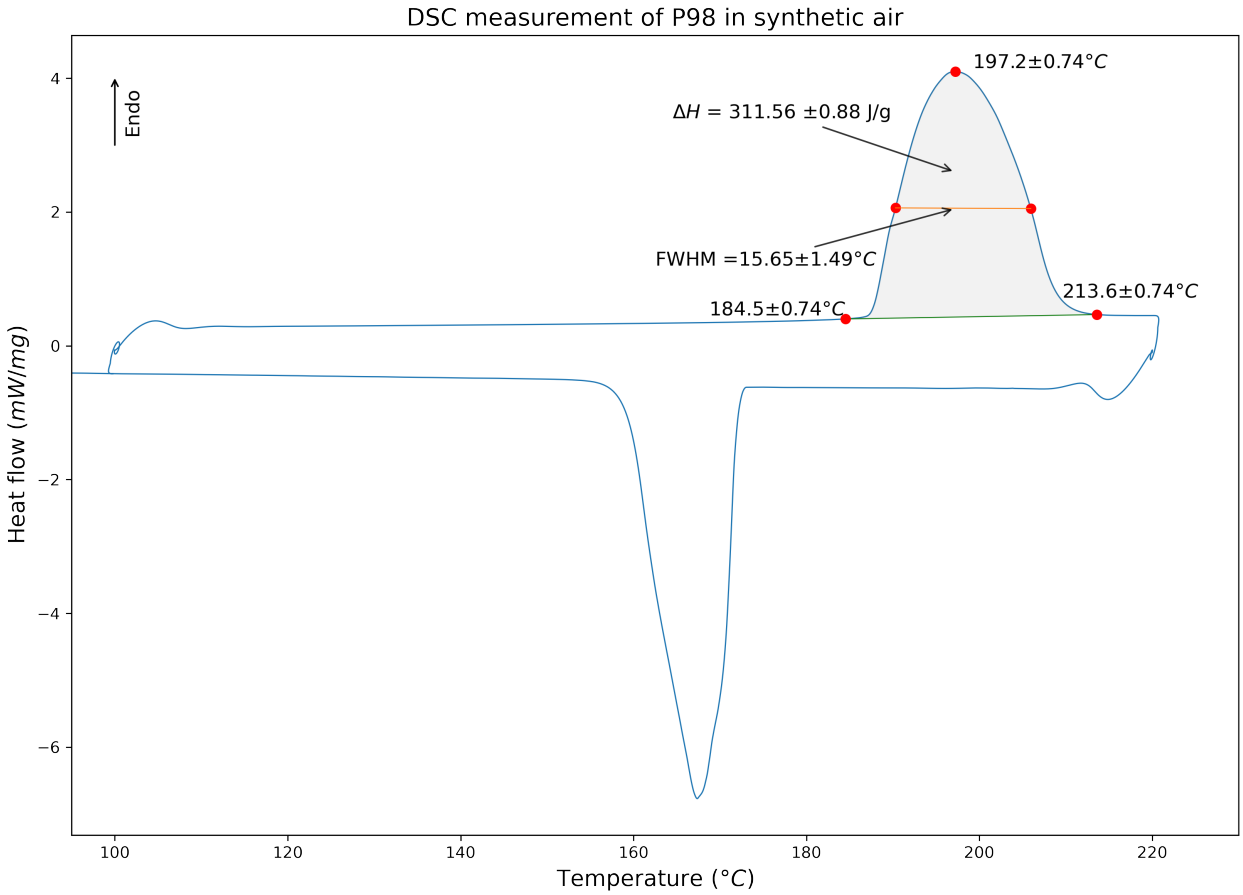

Figure 4.2: Illustration of one of the DSC measurements. Here, the temperatures of interest are marked, and it is illustrated which area corresponds to the ΔH for the endothermic phase change. The uncertainties of the measurements are standard deviations calculated from five parallel measurements of the same sample material.

Figure 4.3 is an illustration of all of the initial DSC measurements on the different samples in synthetic air and argon. The calculated enthalpy of the endothermic peaks is presented in each corresponding plot. The peak areas seem to be larger for the synthetic air measurements than for the argon measurements. The shape of the peaks also varies. From the figure, it seems that the shapes are somewhat similar for the same sample in a different atmosphere. However, when comparing the different samples it is clear that they have some differences in the heat flow curve. The start temperature of the peak seems to vary, and the peak value also seems to happen at slightly different temperatures. The P86 measurements are also particularly interesting. Here, the endothermic peaks have a shoulder. This shoulder is also slightly visible in the exothermic peaks. For this sample, the artifact when starting to heat the material from $100°C$ also seems slightly larger.

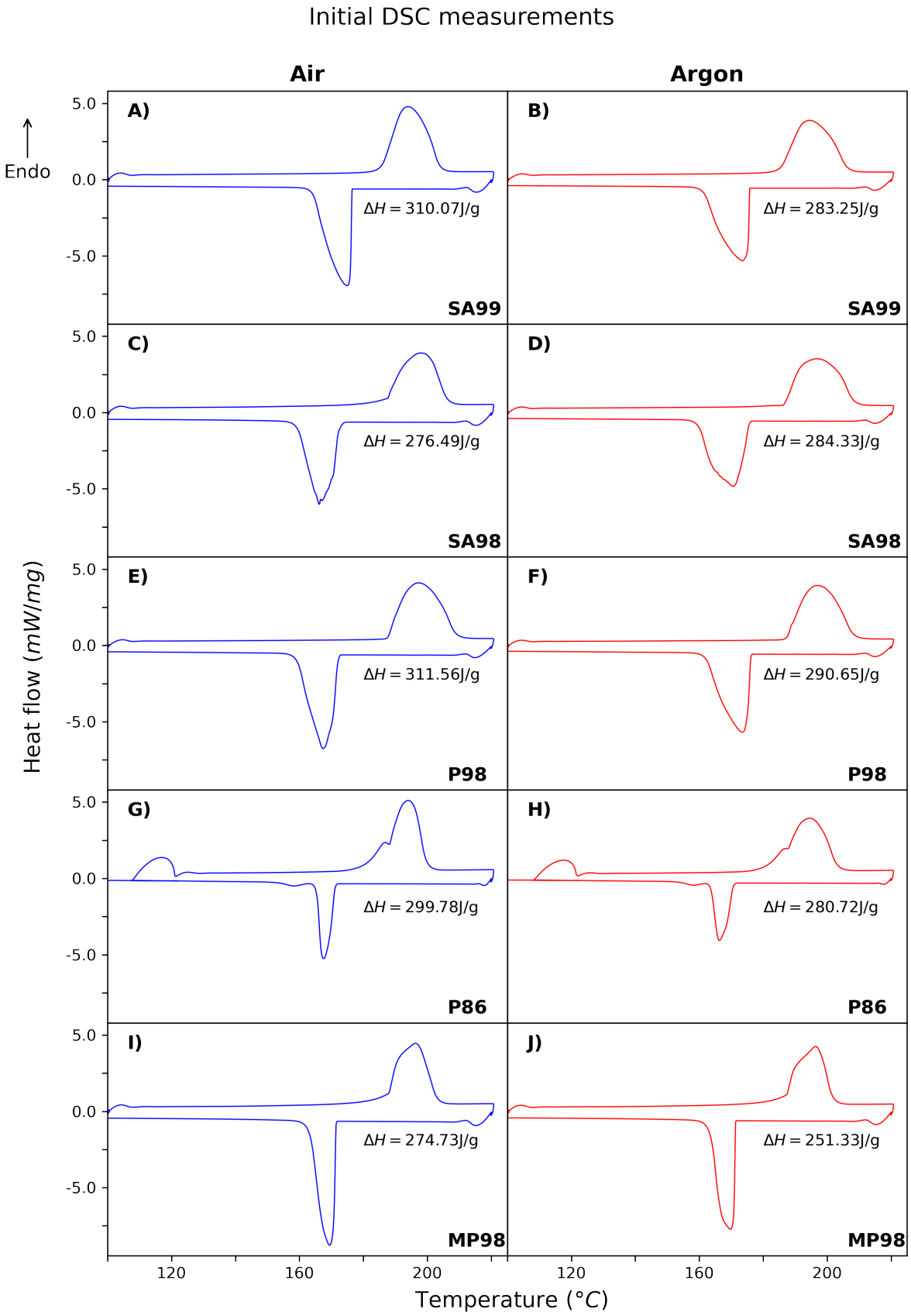

Figure 4.3: Illustration of all initial 2-thermal-cycle measurements. All the samples were tested in both synthetic air and argon. Notice how the endotherm part of each plot has a positive heat flow value, whilst exothermic heat flow is on the negative side.

Table 2 compliments the gathered data from figure 4.3 by stating the values of the most important endothermic peak characteristics being the start temperature, the maximum temperature of the peak (bulk temperature), and the end temperature of the peak. In this table, the difference between the end and the start temperature of each peak, and the FWHM of each peak is also stated. From the presented values, one can observe how the start temperature change. It seems that the starting temperature for each peak except for the MP98 is higher in the argon atmosphere than in the synthetic air atmosphere. The end temperature seems to follow this trend for the most part, but the end temperature of the peak for P98 is also slightly lower in argon than in synthetic air. The bulk values seem to vary quite a bit more. Looking at the difference between the start and end temperature of each peak, there is no pattern to follow regarding the choice of atmosphere. In regards to the sample purity, it seems that a higher purity means a smaller difference between the start and the end of each peak when looking at the two different material providers. The sample MP98, which was the melted sample, interestingly seems to have the largest difference in the start and end temperature of the peak.

Table 2: Start temperature, bulk temperature, and end temperature of the endothermic peaks in the initial DSC measurements are gathered. Furthermore, the difference between this start and end value is stated, and the FWHM for each peak is also found. The temperatures are given in $^{\circ}C$ for all measurements.

	SA99		**SA98**		**P98**		**P86**		**MP98**	
	Air	**Argon**	**Air**	**Argon**	**Air**	**Argon**	**Air**	**Argon**	**Air**	**Argon**
Start	176.61	178.08	171.31	176.81	184.51	184.64	169.58	172.15	164.75	163.04
Bulk	193.88	194.48	198.05	196.71	197.25	197.08	194.04	194.61	196.31	196.41
End	207.78	210.67	210.71	213.14	213.58	213.18	204.28	208.11	207.54	206.61
FWHM	13.3	15.11	15.23	16.77	15.44	14.88	11.55	12.91	14.16	11.35

4.1.3 Thermal cycling measurements

The thermal cycling DSC experiment described in section 3.2.3 involved the thermal cycling of the five samples fifty times in both a synthetic air and argon atmosphere. Here, the enthalpy of every cycle, and the start-, bulk-, and end-temperature for every endothermic peak were gathered. Figure 4.4, and figure 4.5 illustrate the measured enthalpies as a percentage of the enthalpy of the first measurements.

Looking at these results, several observations are made. Generally, one can find that in argon, the enthalpy seems to remain stable around 100% of the initial enthalpy, with a maximum lowering of enthalpy of 1.35% after 50 cycles for sample MP98. In synthetic air, the story is different. Here, the spread between the samples seems to be much larger, and the largest degradation of enthalpy after 50 cycles was seen in sample P98 with a 12.07% decrease. One can also find that in the data for both the synthetic air and argon measurements, cycle number 10 has a higher measured enthalpy than the enthalpy measured at cycle 0. This holds true for all samples except for the P98 sample in a synthetic air atmosphere.

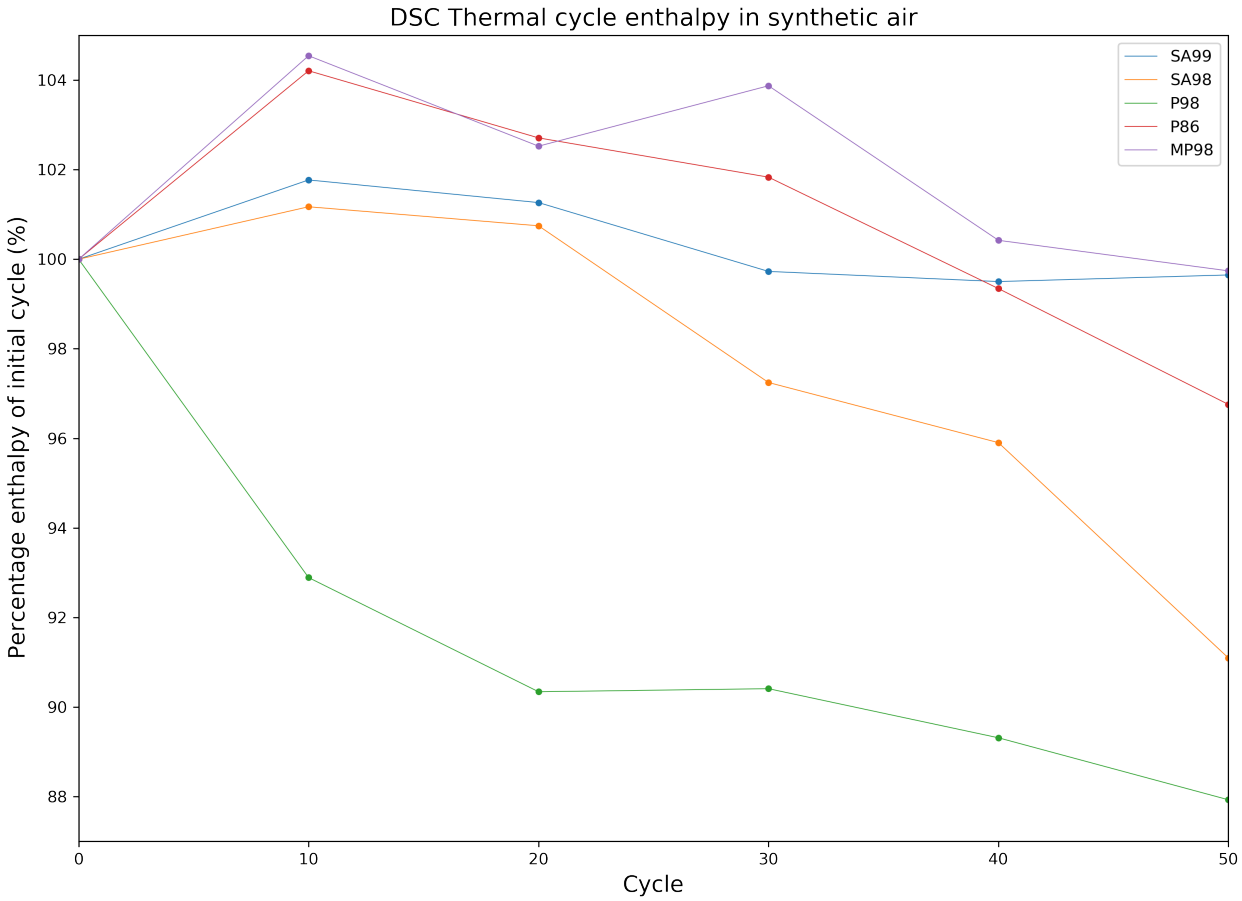

Figure 4.4: Percentages of the initial endothermic enthalpy for every 10 cycles up to 50 total thermal cycles. Measurements made in a synthetic air atmosphere. Five different samples were measured.

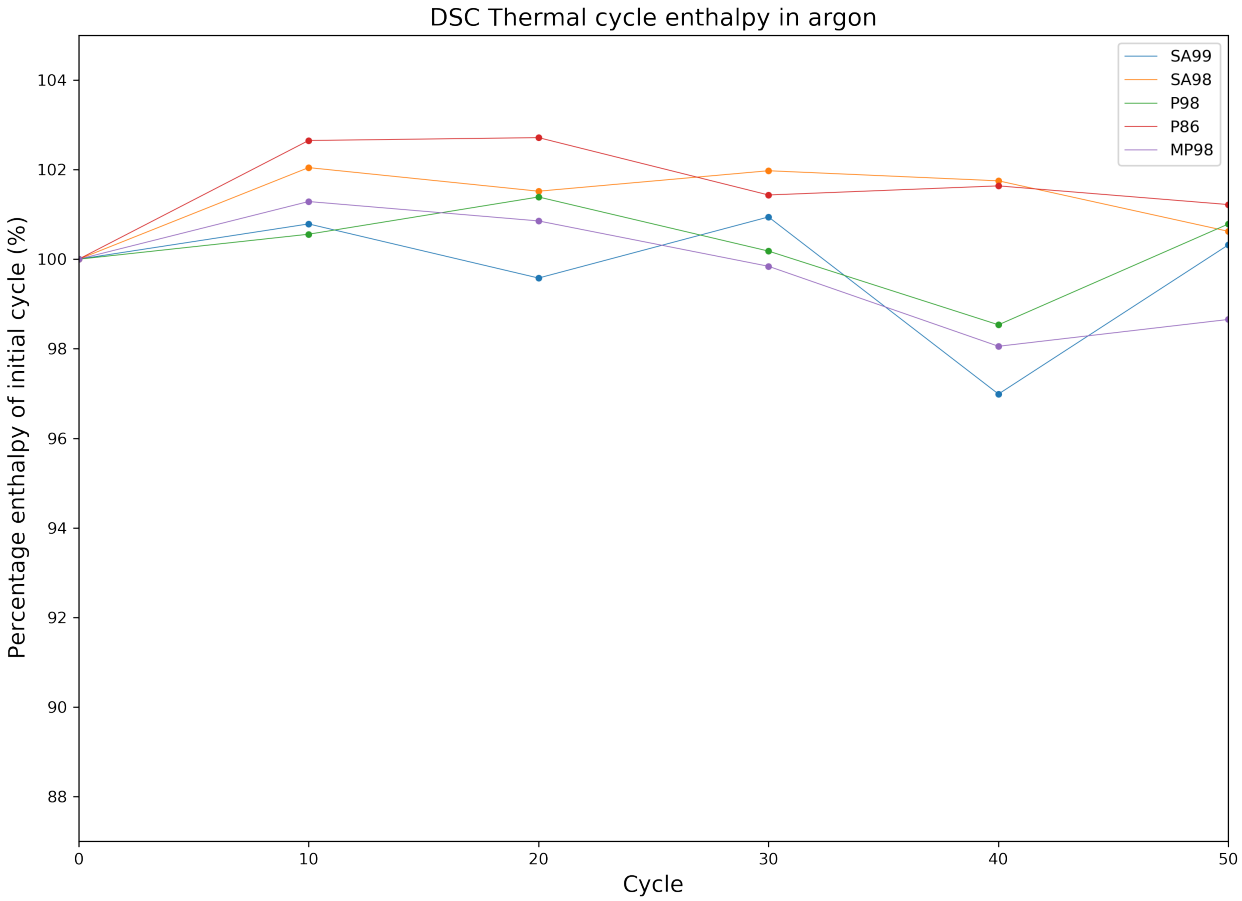

Figure 4.5: Percentages of the initial endothermic enthalpy for every 10 cycles up to 50 total thermal cycles. Measurements made in an argon atmosphere. Five different samples were measured.

The start-, bulk-, and end-temperature for the endothermic solid-solid phase change during thermal cycling can be seen in figure 4.6. Here, all the samples are compared in both a synthetic air and argon atmosphere. From the plots, it is possible to observe how the start temperatures seem to have more noise in synthetic air than in argon. Furthermore, it seems like the start temperatures deviate more in a negative manner from the initial measurement in the synthetic air atmosphere than in argon. For both atmospheres, however, it seems that the end temperature is lowered and that it is coming closer to the bulk phase change temperature. Furthermore, the bulk transition temperature remains somewhat stable for all samples. When looking at the different samples across both atmospheres, it is clear that the SA99 sample seems to remain fairly similar. The SA98 and P98 samples have very different start-temperature for the transition depending on the atmosphere, and the P86 and MP98 samples seem similar in starting temperatures across both atmospheres.

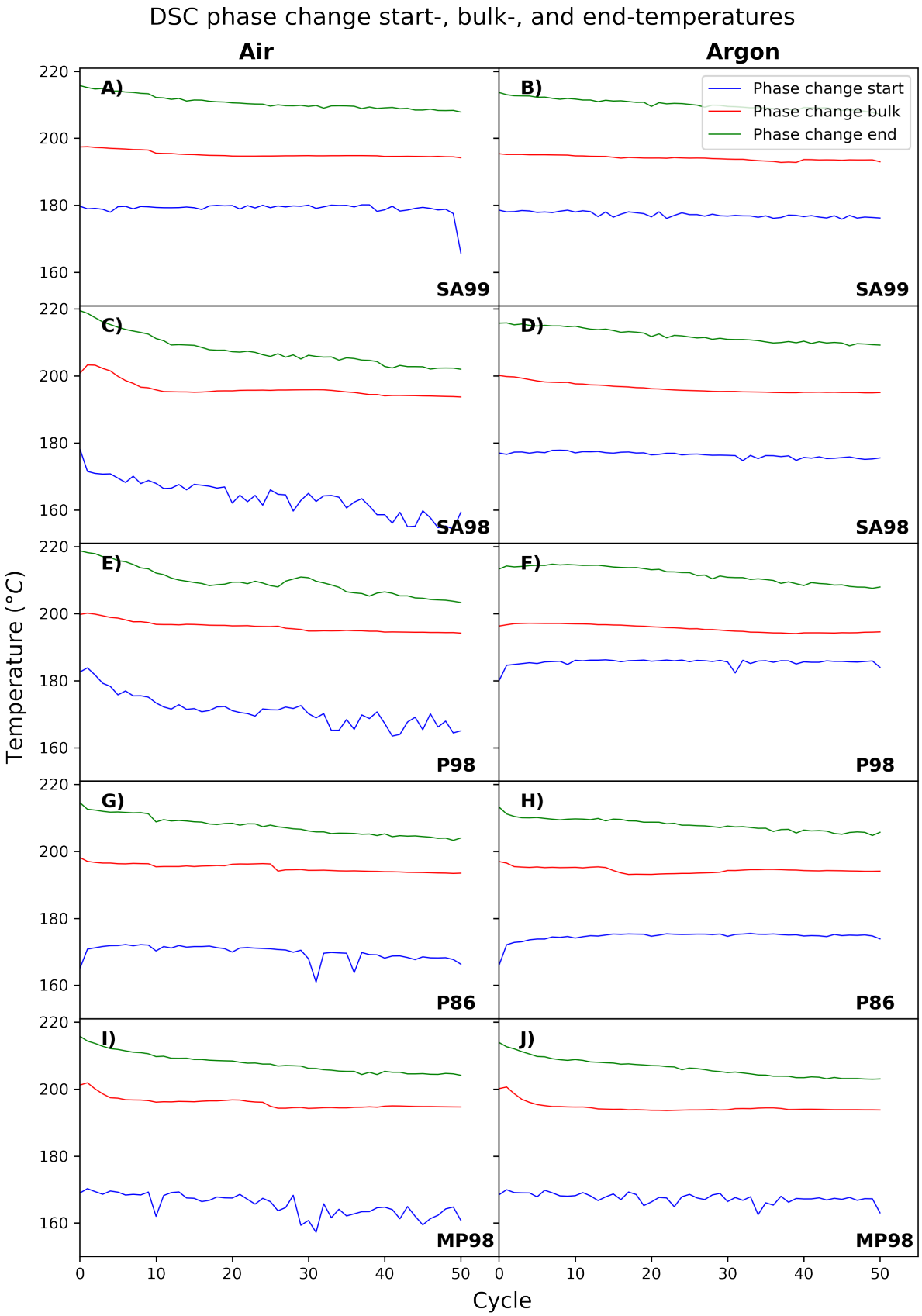

Figure 4.6: Start-, bulk-, and end-temperature for the endothermic solid-solid phase change over 50 cycles for samples in air and argon.

4.1.4 Temperature hold measurements

The enthalpy for the endothermic solid-solid phase change reaction was measured every day during the temperature hold experiment described in section 3.2.4. These enthalpy values are presented in the plot in figure 4.7. Here one can see how the enthalpy decreases until it reaches its lowest value on day 7. From the complimenting table in this figure, the data states that from day 0 to day 7 there was a total decrease in the endothermic enthalpy of 102.33 J/g, which is equivalent to a drop of 37.4%.

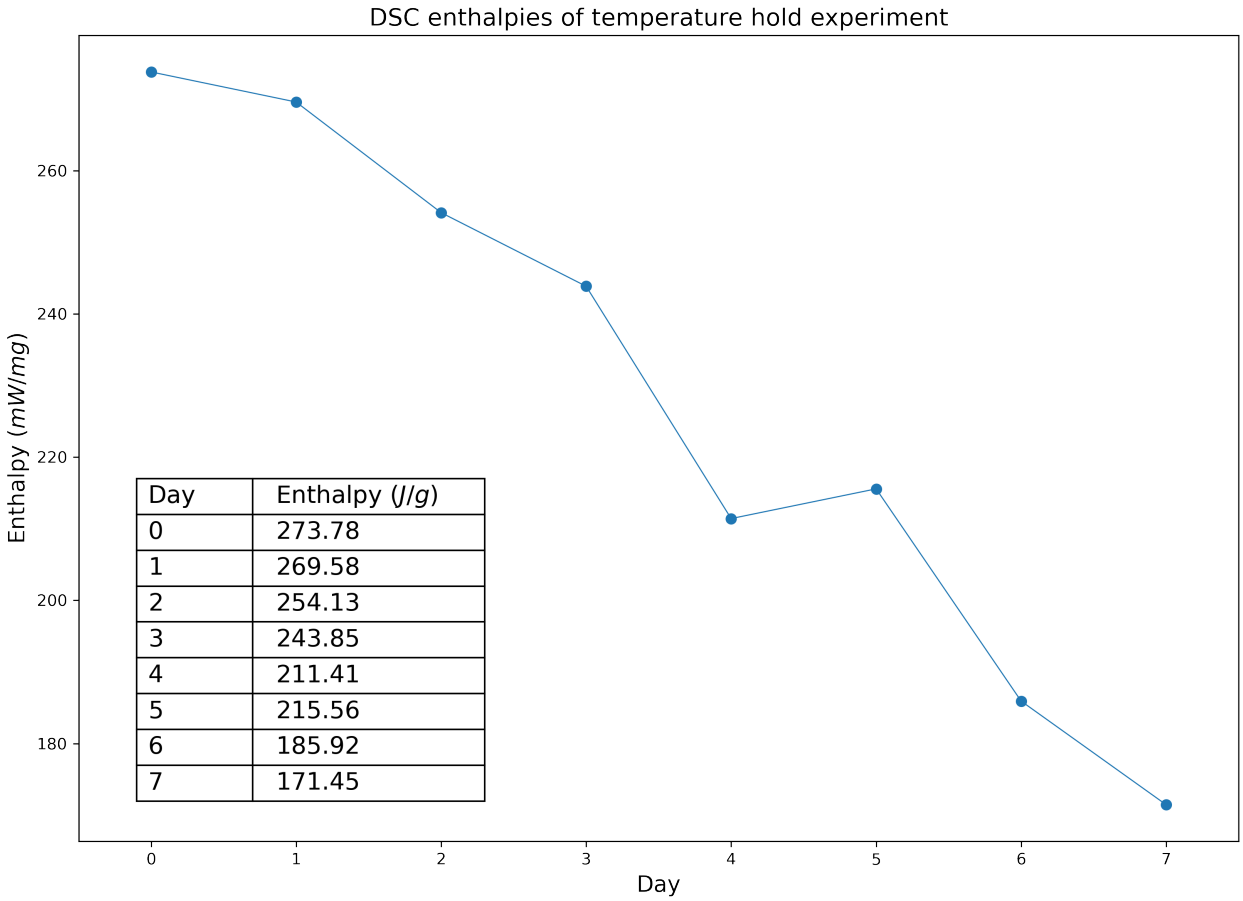

Day	Enthalpy (J/g)
0	273.78
1	269.58
2	254.13
3	243.85
4	211.41
5	215.56
6	185.92
7	171.45

Figure 4.7: Enthalpy measurements for the endothermic phase change in the temperature hold experiment. There is a clear decrease in enthalpy from day 7 to day 0. A table presenting the measured enthalpies is included.

In the same temperature hold experiment, the start-, bulk- and end-temperature of the phase change was determined. This data can be seen in figure 4.8. The start temperature reduces more rapidly than the end temperature and the bulk temperature as a function of days of thermal treatment. The bulk temperature is relatively stable over the seven days with a slight decrease in temperature, and the end temperature is also stable, but the decrease is more noticeable. All in all, there is a broadening in the endothermic peak of the phase change after an increasing amount of days in the oven at 220°C.

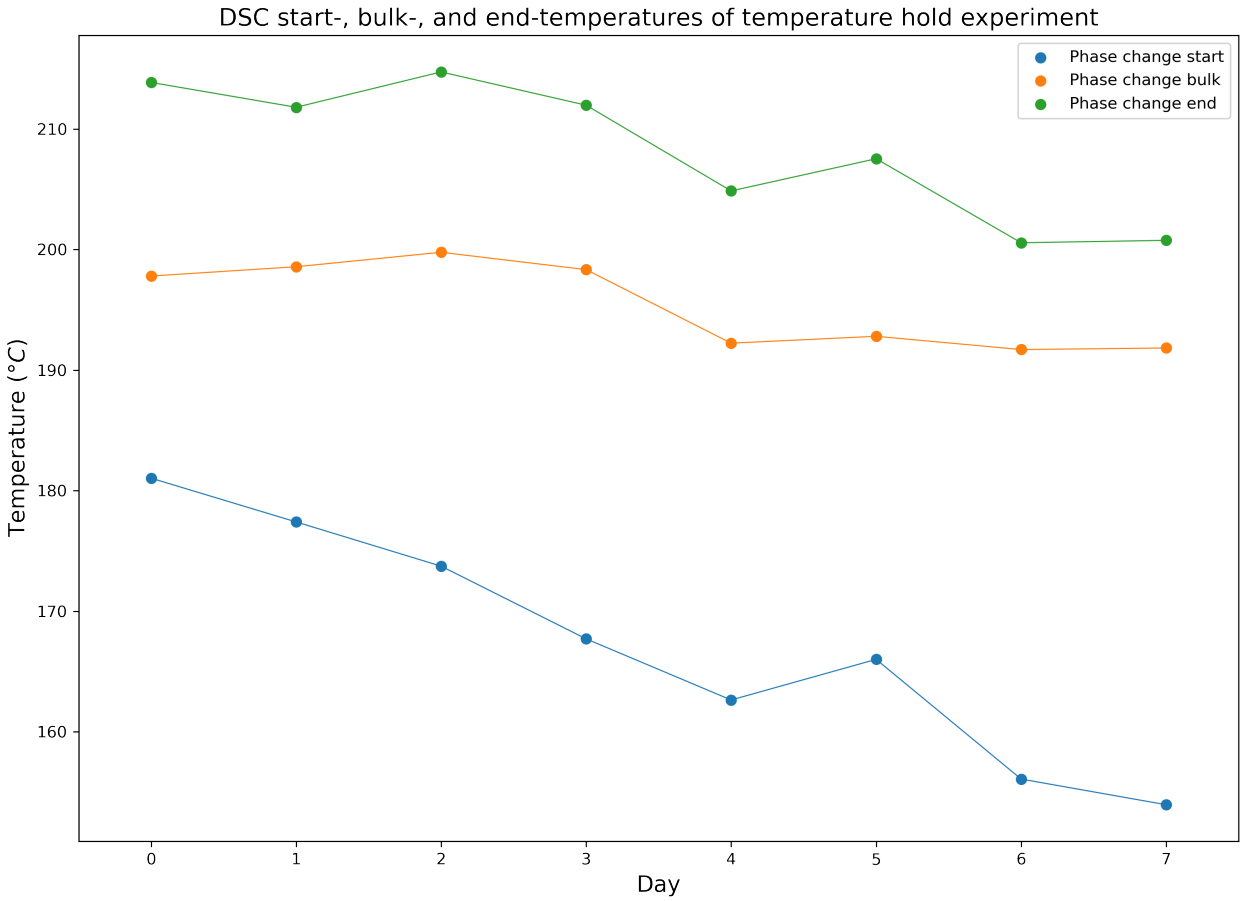

Figure 4.8: Start-, bulk-, and end-temperature for the endothermic solid-solid phase change over a 7-day period from the thermal hold experiment.

4.2 TG and MS

Figure 4.9 is a combination of all the measured values of the TG measurements, as well as the noteworthy MS measurements. In figure 4.9A, one can see how the mass of the material is reduced when the material is heated. The scatter points are the estimated start of the melting point of the material in synthetic air and argon atmosphere. These melting points are estimated from DSC data in figure 4.9B at $256.2°C$ and $260°C$. The indent plot in figure 4.9A is a zoom-in on the start of the mass loss. The synthetic air measurement has a non-typical behavior believed to be a measurement artifact about one-third down in the mass plot. As one can see, the material seems to have been fully degraded and evaporated at approximately $370°C$.

In figure 4.9B, one can observe the measured DSC data during the heating of the material in synthetic air and argon. As indicated, a positive value for the heat flow means that the heat is going into the material, and one has an endothermic reaction. There are three main heat flow peaks visible argon measurements at approximately $200°C$, $270°C$, and $370°C$. The synthetic air DSC measurement has the two first peaks, and the third heat flow peak is split into three. The first and the second of the three peaks coincide with the anomalies in the heating that were also seen in figure 4.9A, so it is believed that these are measurement artifacts. There also seems to be a shorter

segment in the synthetic air measurement where the heat flow is exothermic after the second peak and before the last three.

Figure 4.9C and D are made up of data from the MS measurements. In the first of the two, one can observe the detection of H_2O gas. Here, it seems that the detection starts slightly before the indicated melting point of the material in both synthetic air and argon, and gradually more H_2O gas is detected until the total evaporation of the material. The difference between the measurements in argon and synthetic air pf the amount of H_2O gas detected is significant. There is little detection in the argon atmosphere measurement compared to the synthetic air measurement. The anomaly in the temperature determination for the synthetic air seems to correspond to peak values of the detected H_2O.

This is also evident from the second MS subplot, where CO_2 gas detection is plotted. Here, the detection of CO_2 is close to non-existent in the argon atmosphere measurement compared to the synthetic air atmosphere. The synthetic air measurement has CO_2 gas peaks correlating with that of the H_2O gas peaks, and the DSC heat flow peaks. This is an indication that the anomaly in temperature is messing with the data from the MS. The detection of CO_2 gas in the synthetic air measurement also seems to start slightly before the melting point is reached, even before the detection of any significant H_2O gas.

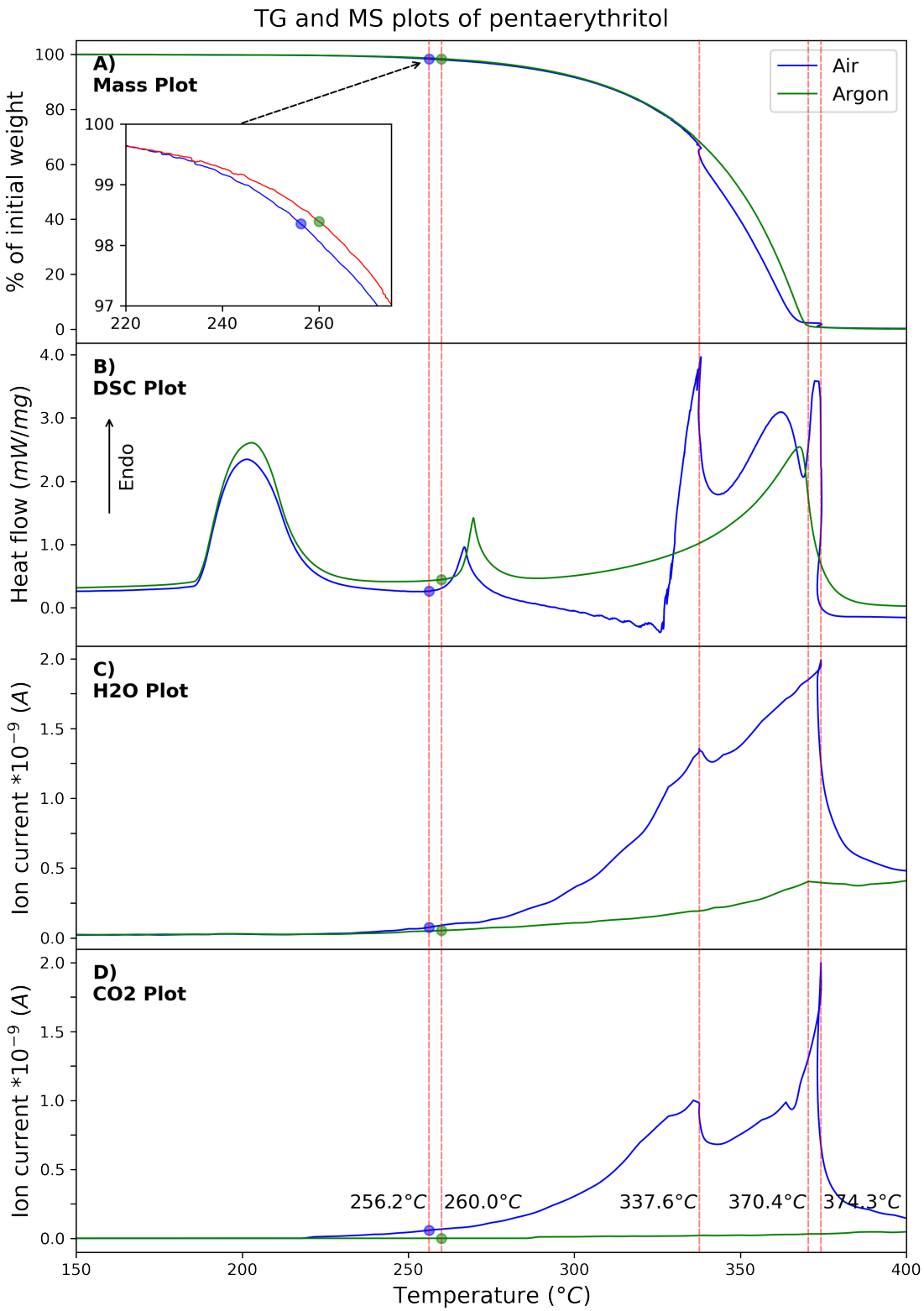

Figure 4.9: Data gathered from TG and MS. All subplots relate the measured data to the temperature. Subplot A shows the recorded weight of the sample. B shows the heat flow. C shows the detection of H_2O. D shows the detection of CO_2. Data from subplot A and B came from the TG apparatus, whilst C and D was found with the MS apparatus.

Figure 4.10 is presenting relevant species detected with the MS. Here one can see the same H_2O and CO_2 detection that was presented in figure 4.9C and D. Other gases that are detected include O_2, OH, CH_2O (formaldehyde), and C. The detection of these gases seems to be more significant in the synthetic air measurements compared to the argon atmosphere measurements. In the air measurements in figure 4.10A, one can see the start and end of the temperature anomaly marked with red dotted lines. Right before, there is a drop in detected oxygen, whilst the other species are increasing. The argon measurements in figure 4.10B seem to have an initial peak for the gases at the red dotted line ($370.4°C$) except O_2 which seems to be decreasing slowly, especially after this peak.

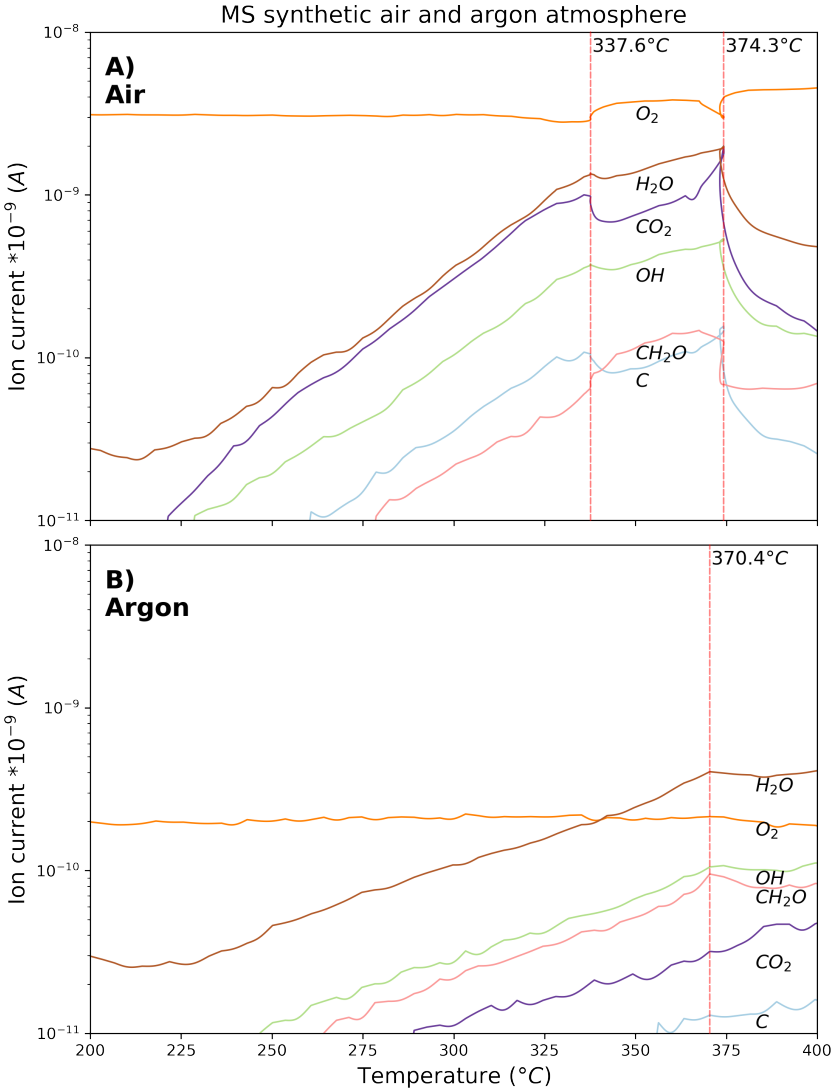

Figure 4.10: Gaseous species detected with the MS apparatus in the TG/MS experiment. Here, the detection of these species is quantified depending on the temperature.

4.3 Laserflash

The thermal conductivity was investigated with laserflash, and the result from the experiment can be seen in figure 4.11. From this measurement, it was possible to determine that the thermal conductivity reduces as the temperature increases. The first measurement at $25°C$ had a mean thermal conductivity of $1.00 \pm 0.04\, W/mK$, and the last measurement before the phase change $175°C$ had a mean thermal conductivity of $0.75 \pm 0.01\, W/mK$. After the phase change, the thermal conductivity seems to drop drastically. At $200°C$, the thermal conductivity can be observed to be as low as $0.32 \pm 0.04\, W/mK$.

A new set of values for the thermal conductivity was found and plotted in figure 4.11 with orange. These values were calculated with equation 2.2, where the C_p found in the specific heat capacity experiment was used. One can see the same trend for both the calculated thermal conductivities, with the C_p from DSC giving slightly lower values ranging from $0.93\, W/mK$ to $0.56\, W/mK$.

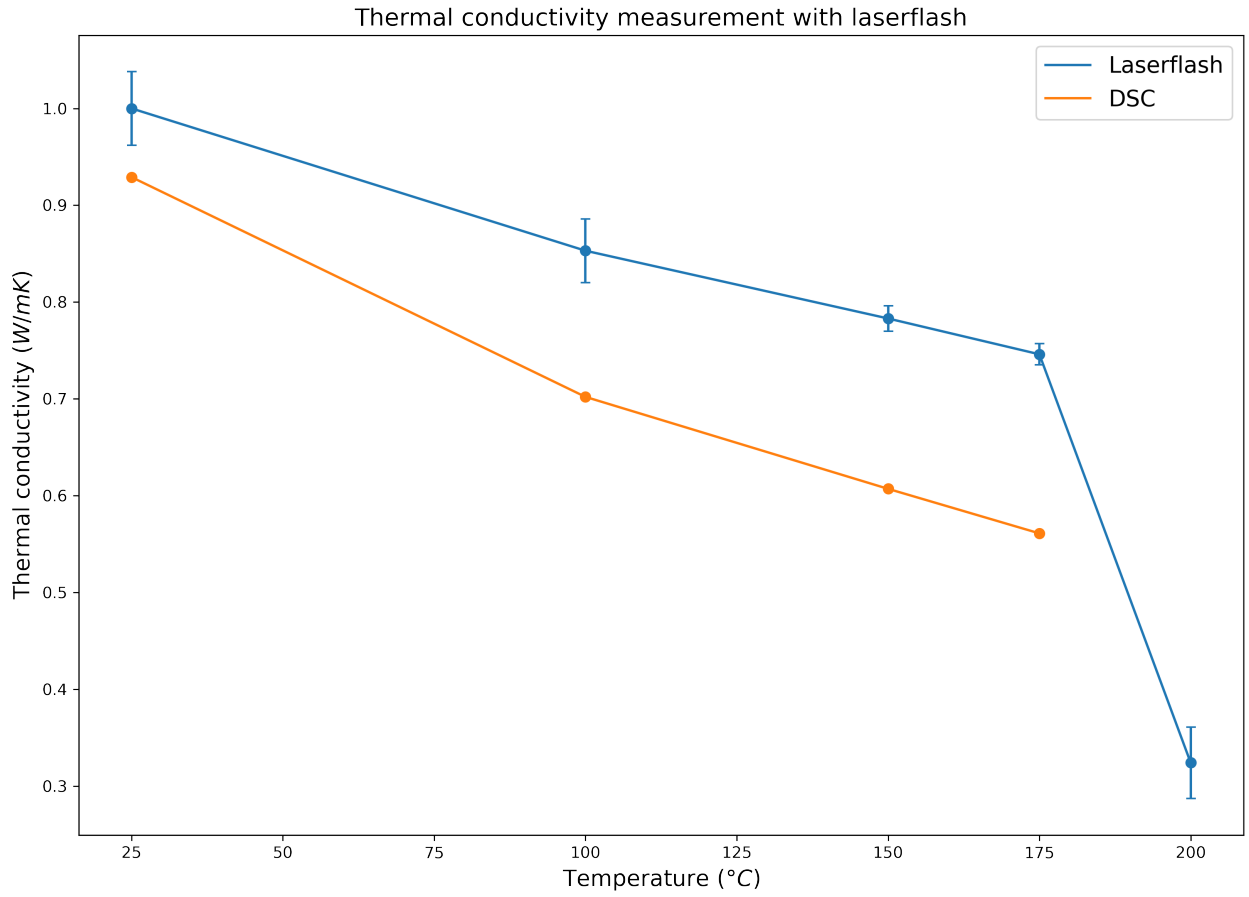

Figure 4.11: Thermal conductivity of pentaerythritol depending on temperature. The blue line represents the thermal conductivity found by the laserflash apparatus. The orange line represents the thermal conductivity found by utilizing the C_p from the DSC and combining it with values found in the laserflash in equation 2.2 to find a new thermal conductivity.

4.4 XRD

4.4.1 Thermal expansion

The first experimental XRD procedure is presented in section 3.4.1, and the results can be observed in figure 4.12. This temperature-dependent XRD analysis is plotted from temperatures between $30°C$ and $185°C$. Results above $185°C$ were left out of the plot as the material had started to melt and sublimate. These results clearly present a general trend of how most of the peaks shift slightly to the left with increasing temperature. There also seems to be a slight decrease in the peak intensity, which is more easily observable in the top right inset plot. Over the entire temperature range, no peaks seem to disappear or to be created. The results were analyzed with the XRD analysis software TOPAS, where the spectra were fitted using Pawley fitting. This enabled the possibility of finding the change in the lattice parameters depending on temperature. The lattice parameters and volume of the unit cell are presented in table 3.

Table 3: Calculations of lattice parameters from Pawley-fitting the data gathered in the temperature-dependent XRD experiment. The acceptable rwp value for the fit was 13.899. The changes in the lattice correspond to thermal expansion coefficients $\alpha_a = 1.72 \cdot 10^{-5}$, $\alpha_c = 15.39 \cdot 10^{-5}$, $\alpha_V = 18.92 \cdot 10^{-5}$ found by utilizing equation 2.4.

Temperature ($°C$)	a (Å)	c (Å)	V (Å^3)	V/V$_0$
30	6.0795	8.7557	323.6130	1.0000
60	6.0791	8.7845	324.6314	1.0031
85	6.0829	8.8213	326.4057	1.0086
110	6.0851	8.8528	327.8010	1.0129
135	6.0875	8.8864	329.3082	1.0176
160	6.0886	8.9185	330.6130	1.0216
185	6.0957	8.9646	333.1027	1.0293

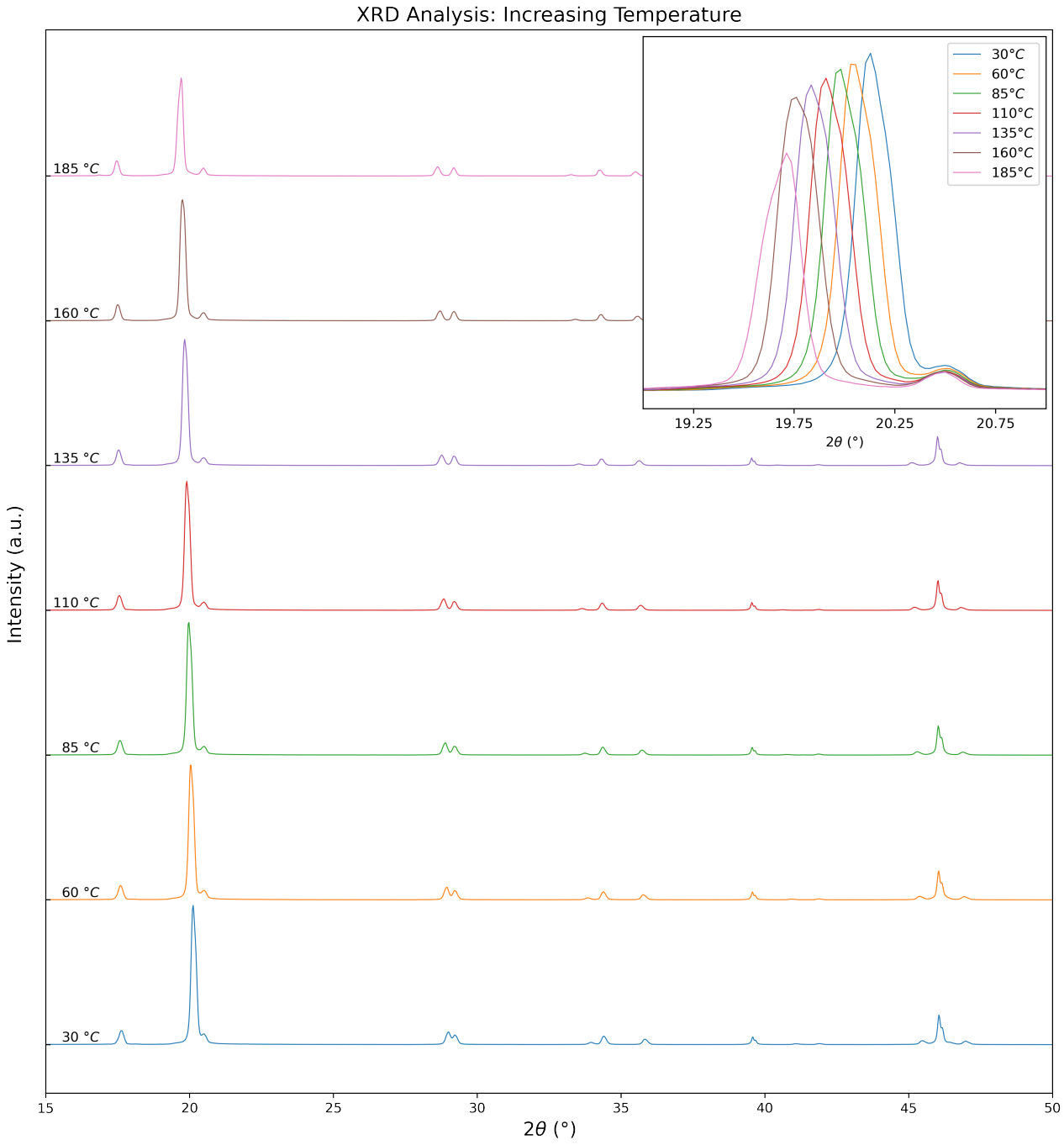

Figure 4.12: XRD spectra of pentaerythritol gathered depending on temperature. One can observe how the peaks change with increasing temperature.

4.4.2 Temperature hold measurements

The results from the temperature hold experiment XRD analysis described in section 3.4.2 are presented in figure 4.13. Here one can observe the XRD measurements conducted before the temperature hold and after 7 days at 220°C. The peaks in both measurements are detected, and the day 0 XRD peaks are indexed. One can observe a reduction in peak intensities, and an increase

in background noise after 7 days. Furthermore, from the peak detection, it is evident that some of the peaks are shifted slightly to the left after 7 days. It is however also possible to see that two of the peaks ((112) and (220)) remain at the same 2θ angle after 7 days of heat treatment. There are also visible shoulder peaks in the day 0 measurements that seem to disappear after 7 days ((110), (020), and (013)). Lastly, peak (004) is missing in the day 7 measurement.

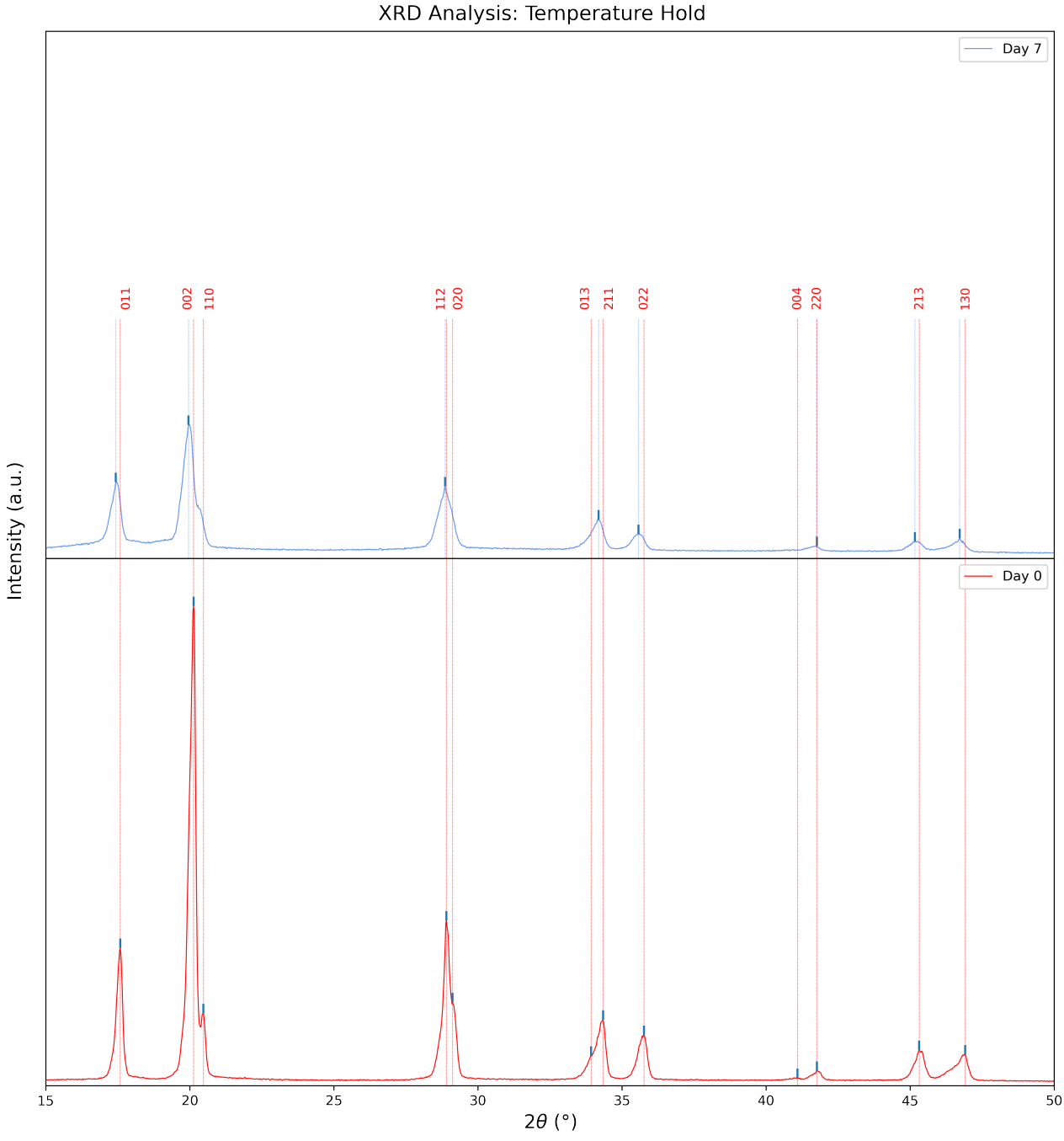

Figure 4.13: XRD spectra from the temperature hold experiment at day 0 and day 7. Peaks are indexed with hkls, and one can observe how many of the peaks shift slightly in the day 7 measurements.

4.5 Raman

The Raman spectra results are presented in figure 4.14, and illustrate the Raman peaks of the P98 sample before melting, after melting and resolidification, and after 7 days of temperature hold at 220°C.

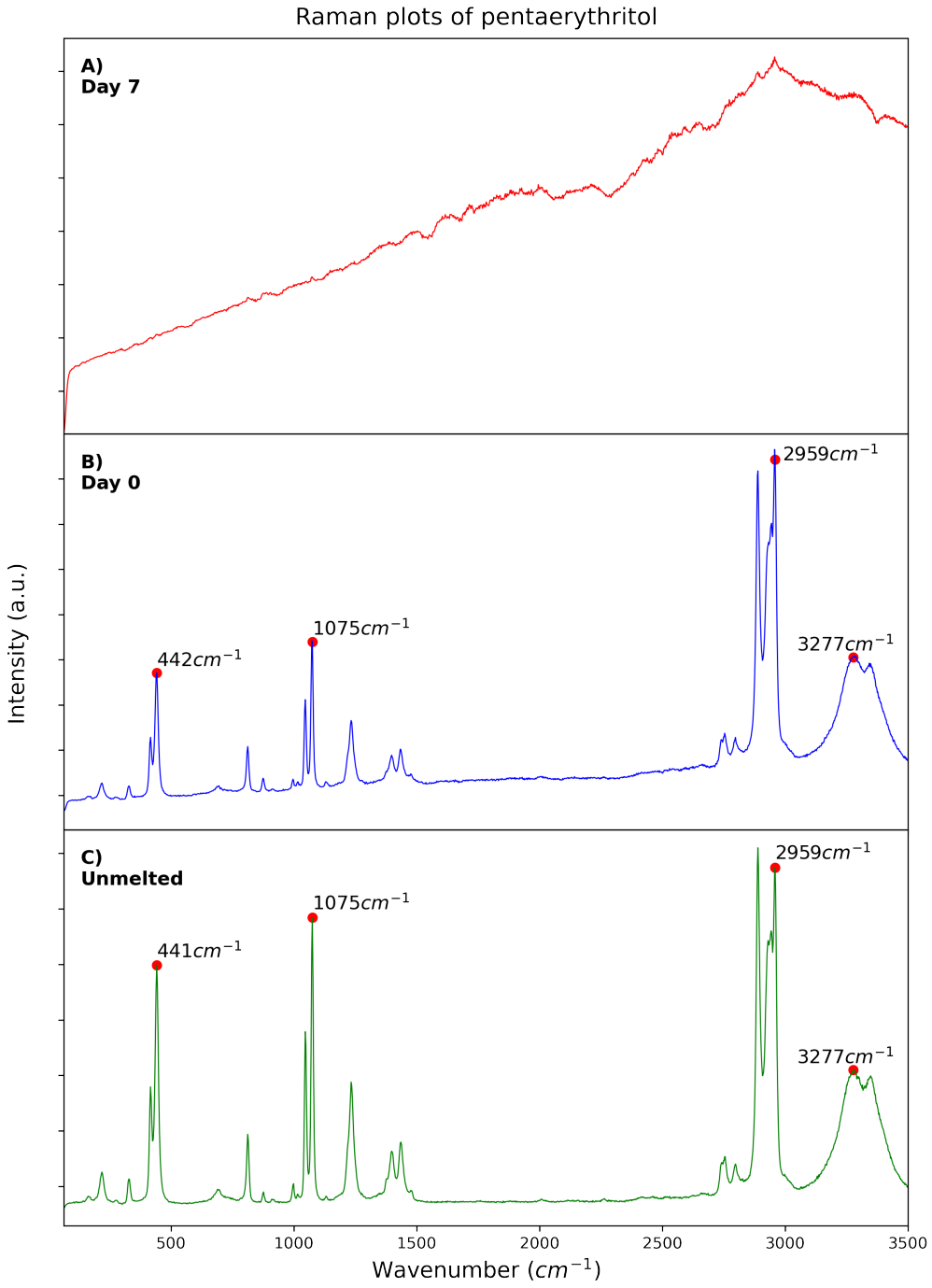

Figure 4.14: Results from Raman analysis before the material was melted and solidified, after the resolidification, and after 7 days in the temperature hold experiment at 220°C. One can observe the same peaks before and after melting. After the temperature hold, there is a lot of fluorescence.

The experimental procedure is presented in section 3.4.3. From the unmelted and day 0 plots, it is possible to observe all of the same peaks. Some of the specific peaks marked for identification are found at the same places for both of the plots. The wavenumber corresponds to different atomic bonds. 442 cm^{-1} (CCC bending), 1075 cm^{-1} (CO stretched), 2959 cm^{-1} (CH stretched), and 3277 cm^{-1} (OH stretched) [52]. For the day 7 measurements, it is harder to detect where the peaks are due to fluorescence, but the highest detected intensity seems to be at approximately the same wavenumber as the other measurements.

5 Discussion

Throughout the investigation of the material's LHS properties, four main areas were in focus. Investigating basic properties necessary for latent heat storage such as specific heat capacity, thermal conductivity, and thermal expansion. Studying if the atmospheric conditions during operation would affect the LHS capabilities of pentaerythritol. Investigating the impact of material purity, and melting and resolidification of the material on the material's LHS capabilities. And to investigate if and how the material would degrade during a temperature hold at the maximum operational temperature. In the following chapter, the experimental results will be analyzed in light of the current research front on latent heat storage materials.

5.1 Basic property characterization

5.1.1 Specific heat capacity

Specific heat capacity plays an important role in TES, and while the enthalpy of change is the determining factor for the amount of heat stored in LHS, specific heat capacity also contributes to the retention of heat within the material. The contribution from the specific heat is pointed out in equation 2.1. This formulation states that both before, under, and after the phase transition, one would have to consider the specific heat capacity of the material, as it is not necessarily the same for all phases. During the phase change, it is important to remember that there are varying amounts of these two phases present. However, for LHS materials, the enthalpy of change for the transition is much larger, making the specific heat capacity negligible. To find the specific heat capacity of the material DSC was utilized. The results of the measurements are presented in figure 4.1. Here, only the BCT phase is investigated, meaning temperatures below the solid-solid phase transition. It is clear from the results that as the temperature rises, the specific heat capacity becomes higher. In other words, more and more thermal energy is needed to increase the temperature of the material. The increase seems significant, going from 1.43 J/gK at 40°C to 2.06 J/gK at 160°C. These values seem reasonable at lower temperatures, as they match very well with previously reported values ranging from $1.55 - 1.99$ J/gK in the temperature interval $60 - 142$°C [42].

5.1.2 Thermal conductivity

To find the thermal conductivity over a set range of temperatures, a laserflash apparatus was utilized as described in section 3.3.1. The results from this measurement are plotted in figure 4.11 with blue lines. Here, the error bars are the standard deviation of the five measurements at each temperature. The general trend for the measurement is that the thermal conductivity seems to become lower as the temperature of the material increases, as expected. After the material has gone through the phase change, the thermal conductivity drops to an all-time low. As the material is heated, the number of active phonon modes increases. This results in a higher chance of phonon-phonon scattering interactions. The disruption of the propagation of the phonons is a direct factor as to why the thermal conductivity becomes smaller with increasing temperature. The second factor that could contribute to the lowering of the thermal conductivity is the motion of free electrons. However, this is not relevant for the current situation, because of the lack of free electrons.

Looking at the values for the thermal conductivity presented in figure 4.11 in blue and comparing them with previously reported values it is evident that the laserflash measurement gave significantly higher values. Previous measurements had a thermal conductivity of $0.66\,W/mK$ to $0.53\,W/mK$ in the temperature range $30 - 180°C$. However, this study also modeled the thermal conductivity, which gave values closer to what was measured, right below $1.00\,W/mK$. It was thought that the model used overestimated the influence of the O−H group [22].

Equation 2.2 explains the relationship of thermal conductivity, thermal diffusivity, specific heat capacity, and the density of the measured material. The values found in the laserflash measurements are presented in table A.3. Here, it can be perceived how the C_p is much higher than the C_p found with the DSC (figure 4.1). Therefore, a new set of C_p values gathered from the DSC experiment was also added to table A.3, and a new thermal conductivity, k, was calculated by using the C_p from the DSC results in equation 2.2. The DSC-calculated thermal conductivity can be seen in figure 4.11 as the orange line. It is clear that the trend seems to be similar, which is a good indication that the relative change is correct. The quantitative values of the calculated thermal conductivity are lower than the values found with laserflash. Here the data presents a drop from $0.93\,W/mK$ to $0.56\,W/mK$ in the temperature range $25 - 175°C$. This was higher than, but closer to the previously mentioned study by Feng et al. [22]. The measured results are however much farther away from the presented thermal conductivity measured by Venkitaraj et al. of $0.106\,W/mK$ [20].

It is difficult to say why the measured values in this study were higher than in previous studies. One reason could be the way the density was measured. Measuring the bulk density only using a caliper and a scale is not as accurate as utilizing the Archimedes principle and finding the apparent density. If the density measured with a caliper was higher, the resulting thermal conductivity would also be estimated to be higher as seen in equation 2.2. Another possible explanation as to why the measured values of the thermal conductivity are higher in this study would be the fact that the pellet was made by melting the material and casting it. This could have minimized the number of pores within the materials, which would be beneficial to the thermal conductivity. In the study mentioned with the lowest thermal conductivity [20], pellets were made by pressing the initial powder without melting it, which could have led to more pores of air effectively lowering the thermal conductivity. The other study [22] had considerably higher values, but here, the material was melted and resolidified beforehand. However, a transient plane source (TPS) technique involving a thermal constant analyzer was utilized, which measures the thermal conductivity differently than the laserflash.

A third reason why the measurements are higher than shown in previous studies could be because of the manufacturing of the pellet itself. By hand-grinding the pellet diameter, the diameter was not perfectly uniform. This could have led to the pellet not covering the entire laser, which could possibly affect the thermal diffusivity parameter, α_{Tdiff} by altering the halftime in the equation 2.3.

5.1.3 Thermal expansion

Previously, the material of sample P98 had been investigated with XRD at room temperature conditions [1]. From this analysis, it was concluded that the space group of the material was $I\bar{4}$. A Pawley fit of the results gave refined lattice parameters of a = 6.1030050Å, c = 8.7856808Å. This fitting was deemed reasonable considering a rwp value of 13.899. This structural determination was in agreement with existing literature [40]. From that initial material analysis, a new temperature-dependent XRD experiment was set up aimed at investigating how the crystal structure of the

material change when the material is heated.

The temperature-dependent XRD investigation of the material was conducted on a pristine SA99 sample, as this was the sample with the highest purity and least likelihood of having other phases present. Figure 4.12 illustrates the measured intensities for the varying temperatures. This was done to investigate the room-temperature crystal structure, the thermal expansion upon heating, and hopefully also the crystal structure of the mesophase of the material. However, temperature measurements conducted above $185°C$ were not presented in these results, as the elevated temperature caused the sample to likely sublimate and melt on the surface, which lead to inconsistent results for the mesophase.

The room temperature structure was refined with Pawley fitting of two structural phases; the pentaerythritol phase, and a secondary platinum phase. When fitting with this model, an initial space group of $I\bar{4}$, and lattice parameters as observed previously were assumed for the pentaerythritol phase. For the platinum phase, the fcc space group $Fm\bar{3}m$ was assumed with lattice parameter a = 0.39236Å[53]. This platinum phase had to be considered, as the sample was deposited on a platinum slide during measurements, and therefore also showed up in the data. It would seem fair to say that the sample and the slide would not react due to the inertness of the platinum. The results from the Pawley fit seemed reasonable with an rwp of 11.463, and lattice parameters of the pentaerythritol phase mentioned in table 1 ($30°C$). In light of these good results, it was considered that one could do fitting of the rest of the data upon heating with these same starting parameters.

When looking at what happens with the XRD spectrum during heating, it is fair to say that some of the peaks from pentaerythritol move considerably. Most apparent is the shift in the peaks on the 2θ-range which the inset plot in figure 4.12 clearly illustrates. This shift can be explained by the lattice change happening upon heating of the material. When the heat goes into the material, the vibrations of the atoms increase, and the distance between the atoms will change. Previous investigations of the bonding in the material concluded that pentaerythritol has weak Van-der-Waals bonds on the crystallographic c-axis, and hydrogen bonds in the (001) planes holding the molecules together [41]. If this is the case, it would be reasonable to say that the Van-der-Waals bonds will break before the hydrogen bonds because of their lower bond energies. This would be observable from the fact that one may see a larger change in the c lattice parameter compared to the two other directions from the XRD results. Table 3 confirms this hypothesis by reporting a lattice change in the c-parameter of 0.2090Å, whilst the change in the a-parameter is a lesser 0.0162Å. Considering this, a total volume increase of the unit cell is reported to be 2.93%. These lattice changes resulted in the thermal expansion coefficients $\alpha_a = 1.72 \cdot 10^{-5}$, $\alpha_c = 15.39 \cdot 10^{-5}$, $\alpha_V = 18.92 \cdot 10^{-5}$ over the entire temperature range. These results correspond well with a beforementioned study by Chandra et al. [46].

5.2 Atmospheric investigations

5.2.1 TG and MS measurements

To investigate the thermal capabilities of pentaerythritol, there was first a need to examine the behavior of the material over the entire temperature range encompassing both room temperature and temperatures surpassing its typical operational range. Therefore an experiment with TG and MS was brought forward. The hope of using an approach described in section 3.3 was that one

would be able to locate the solid-solid phase transition, see when the material starts to melt, see when the material evaporates, find out if there is any amount of sublimation happening, and see when and if there are any gases coming off the sample when it was heated. This data would provide a general understanding of the material over the temperature range, and one could make conclusions as to if the material could be suitable for LHS in the scope of the project. The comparison between running the experiment in an argon atmosphere and a synthetic air atmosphere could put emphasis on whether the atmospheric conditions play a big role in the degradation of the material upon heating.

The first and maybe most important piece of data is the recorded weight of the material during heating. Figure 4.9 illustrate the data captured with TG and MS. From the indent in figure 4.9A, it seems that the initial mass loss in argon happens slightly slower than for the mass loss in synthetic air. This could be an indication that the material degrades faster in synthetic air. Further observation of the entire temperature range in figure 4.9 reveals the weight of the sample until it is fully evaporated. This plot further confirms that the material seems to evaporate faster in synthetic air than in argon. From these results, one could argue that the existence of oxygen is promoting the decomposition of the material. This also corresponds well with previous finds by Zhang et al. [48]. However, what seems like an error in the measurement of the temperature in the synthetic air experiment causes an anomaly in the mass subplot, making it hard to fully analyze these results. This error seems to happen between $337.6°C$, and $374.3°C$, and is likely caused by unstable heating of the material, possibly caused by a big exothermal reaction upon evaporation.

Considering only the mass loss plot in figure 4.9A, it is hard to say exactly when the material starts to melt. However, by looking at the DSC measurement from the TG seen in figure 4.9B, one can make a qualified guess as to where the melting begins. In the plotted DSC datasets, there are several peaks that can be observed. The first peak seems to start at the same temperature for both the argon and the synthetic air runs. This peak is an endothermic peak that is caused by the material going through the solid-solid phase transition. Further DSC data analysis will discuss the size and shape of this peak, and draw conclusions as to what this behavior means. The second DSC peak in this figure is caused by the melting of the material. Previous studies of the material's melting point seen in table 1 seem to coincide very well with the data gathered from the experimental investigation, which is reassuring. The synthetic air atmosphere seems to have a large heat flow increase at $256.2°C$, whilst the argon measurement shows that this DSC peak starts at a slightly higher temperature, $260.0°C$. This further confirms the hypothesis that the material indeed is degrading faster in the synthetic air atmosphere. One could argue that there is a surplus of oxygen in the atmosphere which can react with the material while it is starting to melt and decompose.

When looking at how the mass changes in the indent plot in figure 4.9A, another question arises. Why is there a mass loss before the melting starts? An immediate thought that comes to mind is humidity which is released from the sample upon heating. The humidity could be on the surface of the grains of the sample as well as being trapped within the sample itself. However, above $200°C$, the remaining humidity has likely already evaporated. The H_2O detection with MS can be seen in figure 4.9C. It is shown that there is the detection of water vapor at temperatures above $200°C$ and before the melting of the material, which could indicate degradation of the material caused by surface melting. As previously mentioned in section 2.5.1, surface melting can happen at temperatures below the melting point. It is possible that this surface melting is not perceived as melting in the DSC results because the amounts that melt are so small. If a small atomic layer starts to melt and evaporate before the bulk of the sample, this could be the cause of why gases are

detected before the DSC detects the heat flow associated with melting. A third reason why there is a mass loss could be the sublimation of the material itself. Data from the later thermal cycling DSC investigation supports this theory and will be discussed when looking into the data from this experiment.

The third DSC peak visible in the argon measurement happens at $370.4°C$. This peak corresponds to the vaporization of the material. The DSC peak for the vaporization during the synthetic air measurements is harder to decipher. As previously mentioned, a measurement error in the temperature happens in the temperature range $337.6 - 374.3°C$. This makes it so that it is difficult to trust the DSC and MS measurements in this temperature range for the synthetic air measurements. However, the results are hinting at the heat flow being much greater in the air atmosphere during vaporization than for the heating in argon. This could be explained by looking at the H_2O and CO_2 subplots in figure 4.9C and D. Furthermore, the plot in figure 4.10 includes more of the species detected in the relevant temperature range.

Figure 4.9C states, that the detection of H_2O happens earlier in the synthetic air measurements than what is seen with an argon atmosphere. Furthermore, it seems that the amount of water vapor detected is greater in the synthetic air measurements. This would make sense, as there is more oxygen readily available for the gas evolution to take place. When looking at the H_2O detection in the argon measurements, there seems to be a substantial amount detected. However, this amount is lower than for the synthetic air measurements, and they also seem to happen at higher temperatures. Because of the inertness of the atmosphere, the only gas evolution to take place would emanate from the self-decomposition of the material when higher temperatures are reached. The more significant detection of H_2O in synthetic air atmosphere compared to the inert atmosphere has also been found in previous studies. Here, FTIR analyses showed a much greater detection of $-OH$ in a synthetic air atmosphere compared to a nitrogen atmosphere [48]. This points towards the conclusion that the material degrades more rapidly when in contact with oxygen. Data from CO_2 detection with the MS seen in figure 4.9D also supports this claim. There is a much more substantial amount of carbon dioxide detected in the synthetic air experiment when compared to the argon measurements.

When thinking about how the material degrades, all molecular weights detected in the MS are important to consider. This data is plotted in figure 4.10. When looking at the synthetic air measurement in subplot A, it is important to recognize that although there is some error in the temperature control of the heating cycle that affects the measurement it is still possible to see that there is a good indication that oxygen contributes to the greater amounts of gaseous species found here compared to the measurements in the argon atmosphere in subplot B.

It is possible that when the material degrades $-OH$, $-H$, $-C-$, and other species will react with the surrounding atmosphere, and one could create gases such as H_2O, CO, and eventually CO_2. If the atmosphere consists of synthetic air, it may be speeding up this degradation since the material can bind its atoms to O_2 in the surroundings. In the argon measurements, however, the atmosphere does not have any species that will allow this gas evolution to happen faster, which could lead to the melting point being slightly higher. Previous studies with FTIR spectroscopy have shown the detection of both H_2O, and CO_2 when heating the material in air [48].

A study on the degradation of pentaerythritol in swelling intumescent paints also suggested the formation of formaldehyde upon the increasing temperature in an acidic environment illustrated in figure 2.3. In both the synthetic air and argon measurements, formaldehyde was detected (CH_2O), which is an indication that this might be one of the decomposition products [50]. Other hydrocarbons such as acetaldehyde (C_2H_4O), methane (CH_4), and methylene (CH_2) overlap with

the corresponding molecular weights of carbon dioxide (44), oxygen (16), and nitrogen (14), making it impossible to distinguish from the measured MS data because of the constant gas flows. However, this does not mean that they are not here.

Lastly, it is also worth mentioning that there could be other, heavier, decomposition products formed when PE is degrading that was not detected with the MS due to the high molecular weight. Two possibilities are seen in figure 2.2. As the hydrogen is released and creates H_2O, pentaerythritol molecules could have bonded to each other creating dipentaerythritol and [3,7,7-tris(hydroxymethyl)-1,5-dioxocan-3-yl]methanol [49].

This detection of gases before melting occurs is a clear indication that there is indeed degradation of the material that happens before the melting sets in. This trend seems to happen to a greater extent when oxygen is present in the atmosphere.

5.2.2 DSC measurements

The second set of measurements conducted to analyze the material's behavior in synthetic air and argon atmosphere was done with the help of DSC. The five different samples were initially investigated as described in section 3.2.2. The results from these measurements can be found in figure 4.2, figure 4.3, and table 2. In the first figure, the endothermic peak from the solid-solid phase change of the second thermal cycle of the P98 material in synthetic air is presented to visualize how the data from all DSC measurements was found. The characteristic start and endpoints of the peaks were estimated by utilizing a Python script where the threshold for start and end was set to $3 \cdot 10^{-4}$ for the derivative of the heat flow. Having this threshold set for all the measurements made it possible to compare the results of every cycle. The exothermic phase transition was not investigated as thoroughly, because the thermal cycling measurements described in section 3.2.3 did not have sufficient cooling for the material to cool linearly. However, the general characteristics of these peaks are open for discussion.

The standard deviation presented in figure 4.2, comes from five one-cycle measurements done on five samples of the same material. Here, the endothermic enthalpy was found for each sample, and the standard deviation was found. This standard deviation for the enthalpy is the one seen in the figure mentioned. Furthermore, the other points of interest (start, peak, end, and FWHM points) were also analyzed and a standard deviation from a combination of all of these points for all the samples was found. This is the deviation of $\pm 0.74°C$ that can be seen. The FwHM is a doubling of this value, as both the end and the standpoint for the FWHM have their own standard deviation.

When comparing the characteristics of the initial DSC measurements in synthetic air and argon atmosphere, seen in figure 4.3, it is evident that the ΔH is smaller for the argon measurements than for the measurements conducted in synthetic air. A possible explanation is found in material degradation. From the previously analyzed TG and MS data seen in figure 4.9 and figure 4.10, almost no gases were detected in the temperature range of the solid-solid phase transition. However, it does seem like there might be a small amount of gas being produced at the end of the solid-solid transition in the synthetic air atmosphere, which could indicate that there is a small amount of surface melting happening. This degradation and creation of new species would likely require more energy, which could explain the higher enthalpy values for the synthetic air measurements.

The thermal cycling measurements in figure 4.4 and figure 4.5 illustrate how the enthalpy changes as

a percentage of the initial enthalpy of the material when the samples are cycled thermally 50 times. When these results are compared with respect to the atmosphere it is apparent that the samples seem to degrade faster in synthetic air. This supports the claim that there is some degradation going on even under the melting point of the material, which would mean the production of new species like gases such as CO_2, and H_2O. It is also plausible that variations in instrumental configuration, such as temperature calibration, could have influenced the measured heat flow when operating under different atmospheric conditions.

There is also a possible explanation as to why the material seems to have a higher heat flow peak for the solid-solid phase change in synthetic air for the initial DSC measurements. This would be because the atmosphere also needs to be heated. If the difference between heating the air and heating argon is big enough, one would see some difference in the DSC plots. As known from the literature, the specific heat for air under constant pressure at room temperature is 1.005 J/gK, and 0.5203 J/gK for argon [54]. However, without having any phase changes in the atmospheric gases, the only contributor to the heat flow would be because of the specific heat capacity of the gases. This specific heat would be significantly smaller than the heat needed to drive the phase change itself, and would rather be a part of the background. This background is subtracted from the integration under the heat flow curve when estimating the enthalpy of transition. Therefore, it is reasonable to say that the specific heat of the atmosphere doesn't play a role in this difference in enthalpy, but it can play a role in the height of the solid-solid phase change peak.

Shifting focus from enthalpy to other characteristics of the phase change, such as the start temperature, end temperature, and peak temperature where the bulk of the material undergoes change, reveals interesting differences between the synthetic air and argon atmosphere measurements. FWHM measurements for the initial DSC measurements were also found. Values from table 2 tell a story of these important thermal parameters for the solid-solid phase change. The start temperature of the phase transition seems to vary slightly between the samples for the synthetic air and argon atmosphere measurements, but there does not seem to be much of a trend here. From these results, it would be reasonable to say that the atmosphere itself has little to no impact on the starting temperature of the solid-solid phase change in virgin material. This also seems to hold true for the bulk and end of the phase change. Regarding the FWHM of the peaks in synthetic air and argon, there is no conclusive evidence that proves any type of trend regarding the variation in atmospheric conditions.

The second stage of analyzing if the material's LHS properties differ in synthetic air and argon focused on the operational lifetime of the material. For this reason, the thermal cycling DSC program described in section 3.2.3 was created. The goal was to see if the material's LHS properties such as the enthalpy of transition, and other characteristics of the solid-solid phase change would worsen when the material goes through the phase change numerous times. Figure 4.4, and figure 4.5 show the results from cycling the material through the solid-solid phase change 50 times. Because of the difference in the enthalpies, these results are presented in a percentage of the initial measurement. This makes it easier to compare the significance of the change of enthalpy. Furthermore, figure 4.6 presents the characteristic points for the phase change temperatures such as the start of the transition, where the bulk is transitioning, and the end of the transition.

Comparing the enthalpy plots for cycling in synthetic air and argon atmosphere seen in figure 4.4 and figure 4.5, it is noticeable that when the material is thermally cycled in synthetic air it seems to degrade significantly more on average for the samples as compared to the samples thermally cycled in argon. This finding further contributes to the hypothesis that even though the measurements are

made below the melting point of the material, some degradation is happening, and more so when the heating is done in the presence of oxygen. As mentioned several times, surface melting could be a major factor that is contributing to this degradation. After 50 cycles, the sample with the most degradation in enthalpy in the argon atmosphere saw a decrease by 1.35% from the initial value, and for the synthetic air measurements, the sample with the most degradation was as much as 12.07% decrease. To draw a conclusion about the degradation of the enthalpy in regards to the operational lifetime it would be necessary to conduct more thermal cycles to see if these trends continue.

Interestingly the data in figure 4.4 and figure 4.5 suggests that for all the samples, except for P98 in synthetic air, there is an increase in enthalpy from cycle 0 to 10. It is difficult to say why this is the case, but one explanation would be the error in the measurement. However, the error was determined by testing 5 samples of one purity, and then making a standard deviation of these samples. This error for the enthalpy variation is not visible in the plot, as it was estimated to be as little as $\pm 0.88\ J/g$, corresponding to a very small percentage of the initial enthalpies. Another possible explanation could be that the material somehow starts to recrystallize differently in the early stages of thermal cycling. Maybe sample impurities slowly start to create new species, which could increase the enthalpy of change slightly.

When carrying out the thermal cycling with DSC, the sample weight had to be measured every 10 cycles. Table A.2 presents the fractional parts of the initial weights for all the samples measured in synthetic air and argon. This was necessary to do because of the utilization of pierced-lid sample crucibles. From this table, it is evident that there is a significant mass loss upon thermal cycling. The most likely explanation is that the material is sublimating already at the solid-solid phase change. This loss of material below the melting point needs to be prevented by having a closed atmospheric system.

When it comes to the start, bulk, and end temperature of the phase change during the thermal cycling, seen in figure 4.6, it is apparent how the start temperature is decreased in synthetic air whilst it remains more stable in argon. This decrease could again be an indication of material degradation. This trend is also slightly present for the end temperatures, whilst the bulk transformation temperature seems to remain stable in both atmospheric conditions. It is also noteworthy to mention how the synthetic air measurements in figure 4.6 seem to have more noise for the starting temperatures. A possible explanation is that because of varying amounts of surface melting happening, there are slightly different temperatures for the starting points. In the argon atmosphere, there is no oxygen, which makes it so that the surface melting does not happen to the same degree, and therefore the starting temperature remains stable.

5.3 Purity and melted sample investigations

One of the main challenges to overcome was to find out if a lower-purity material would live up to the properties required for LHS. A lower purity would mean a lower material cost, which would enable the production of cooking stoves for a lower price. To overcome this challenge, the experimental procedures were targeted at investigating this. Five samples of three different material purities from two suppliers were investigated. One of the samples was made up of pre-melted material from the P98 sample. DSC and Raman results help to draw a conclusion as to if and why the material purity matters for the desired application.

5.3.1 DSC measurements

As mentioned in section 5.2.2, initial DSC measurements were conducted on all the samples in synthetic air and argon. The experiment aimed to explore potential variations in the enthalpy change and phase change characteristics, such as the transition's starting and ending points, by conducting the study under different atmospheres. Additionally, the investigation aimed to examine the potential impact of material purity on the LHS properties of the material. Figure 4.3 presents the initial DSC measurements for one thermal cycle.

The enthalpy of change is largest for the P98 sample, but very similar to the SA99 sample. The two lower purity samples SA98, and P86 both have a lower enthalpy of change. However, it seems like the P86 sample can store considerably more energy in the phase change even though this is of a lower purity (86%) than the SA98 sample (98%). The last sample was the melted MP98, which had the lowest enthalpy of change. Comparing the results from the samples measured in argon, it is safe to say that there are some similarities to the synthetic air measurements. The P98 sample is still the one with the highest enthalpy of change. After that, SA98, SA99, and P86 all have a very similar enthalpy of change. Lastly, the melted MP98 has the lowest enthalpy of change by a longshot. If one compares sample purities from the different providers, there is a clear pattern for the Perstorp samples (P98, and P86), which points towards the fact that a lower purity means a lower enthalpy of change. The Sigma Aldrich provided samples (SA99, and SA98) also follow this behavior in synthetic air, but in argon, the samples seem to have about the same enthalpy of change. These different trends between the providers could be explained by different types of impurities in the samples. As known, dipentaerythritol is a frequently found impurity in pentaerythritol together with formaldehyde. Supplier Perstorp reported up to 8% dipentaerythritol content in sample P86, but did not disclose any specific impurities in sample P98. Both samples from Sigma Aldrich did not disclose any specific types of impurities. Because of this, it is hard to find any conclusive evidence regarding samples SA99 and SA98, but the difference in enthalpy between samples P98 and P86 could be explained by the impurity content. When it comes to the melted and resolidified sample MP98, it is very clear that the degradation during melting is what has led to the reduction in enthalpy.

An interesting observation made in figure 4.3G and H is that of the sample P86. Here, the data suggests that there is a splitting of the peak of the heat flow for the endothermic solid-solid phase change that is uncharacteristic for the material. A possible explanation for this could be the higher amount of impurities, here mainly dipentaerythritol. It is uncertain whether the splitting is caused by a phase change in the impurity itself, or if the impurity impedes with the phase change of pentaerythritol, causing this behavior.

Table 2 displays how the characteristic temperatures for the phase transitions vary. Here it is safe to say that for higher purity and unmelted material, there is a higher starting temperature for the phase transition when dividing the sample providers. Furthermore, the Sigma Aldrich samples (SA99 and SA98) show a lower bulk transition and end transition temperature for the higher purity sample. This means that for the higher purity sample, the transition also happens faster. This is evident by looking at the FWHM of the Sigma Aldrich samples. This is not the trend for the Perstorp samples, however, and it makes it hard to conclude how much the purity and resolidifying of the material affect the speed of the transition. In the same table, the full-width-half-maximum (FWHM) values are also presented. In this case, the FWHM is a measurement of how fast the solid-solid phase change happens. The data from the Sigma Aldrich samples suggests that the higher the purity, the faster the transition. The same conclusion could not be drawn for the Perstorp

samples. It does make sense that the transition would go faster when there are fewer impurities present, as any impurities can introduce defects in this lattice structure, making it more difficult for the material to transition through the phase change.

The last DSC investigation done with regard to purity was the thermal cycling of the material. Figure 4.4 and figure 4.5 displays the enthalpies of transition for every 10 cycles relative to the starting enthalpy, and figure 4.6 illustrates the key temperatures associated with the phase changes. The goal of this cycling was to see if the purity and resolidification of the material would affect the effective lifetime of the PCM. From the first two plots, it is not possible to say if the degradation in enthalpy can be linked to the purity of the material. The third plot showcasing the characteristic temperatures of the phase transitions gives some indication that the starting temperature changes more for lower purity samples (SA99 and SA98 in air), but it is not conclusive enough.

5.3.2 Raman unmelted vs melted

The Raman measurement was mainly done to map any changes in the temperature hold experiment. However, an unmelted sample of P98 was also tested before melting it. It is possible to compare the Raman spectra from before and after melting in figure 4.14B and C. Here, all the same peaks are present before and after melting. The only difference between the sample is the background noise. This background noise could be caused because a small number of fluorescent species are created upon melting of the material. One common type of organic material that is known to have fluorescence in Raman is aromatic compounds. Without knowing exactly what types of organic degradation products are produced during melting, it is possible that some of these molecules have been created.

5.4 Temperature hold analysis

The thermal cycling of the material in DSC looked at how the phase transition itself affected the degradation of the material's LHS properties, but it did not investigate if it was the high temperature itself that affected the degradation of the material. The temperature hold experiment was constructed in order to investigate how holding the material at the maximum temperature ($220°C$) for 7 days would affect the LHS properties.

5.4.1 DSC measurements

After every 24 hours, the material was analyzed with the DSC apparatus in an argon atmosphere in order to detect if the properties of the solid-solid phase change had been affected by the heat treatment. This program is described under section 3.2.4. The results from the analyzed enthalpy change of the transition can be found in figure 4.7. It is clear that the enthalpy had been reduced by 37.4% after 7 days. Comparing these results with the results from the thermal cycling (figure 4.4, 4.5), it looks like the maximum temperature hold plays a much more substantial role in the degradation of the enthalpy, and consequently, the material. As mentioned earlier the TG measurements estimated the melting point of the material in argon to be $260°C$. However, it was also clear from the MS data that some gases were detected before this point. Keeping this in mind

when looking at the temperature hold DSC results, it is not unexpected to see this correlation of degradation. The material seems to degrade even before the melting point is reached, which is something that the temperature hold experiment confirms. If this indeed is the true degradation of the material when it is held within the temperature range ($220°C$), one would not be able to approve this material for thermal storage. However, lowering the maximum operating temperature of the material, or having an inert operational atmosphere could change this.

Figure 4.8 presents the start-, bulk transformation, and end-temperature for the DSC measurements from the temperature hold experiment through the seven days. It is clear that the starting temperature of the phase change is decreasing a lot. Degradation of the material seems to lead to a lower temperature for the solid-solid phase transition where the end- and bulk transition temperature decreases slower than the temperature at the start of the phase change. Comparing this with the results from the thermal cycling seen in figure 4.6, one can conclude that the temperature for the endothermic phase transition also seems to change more depending on the temperature rather than going through multiple thermal cycles with shorter holding times at a high temperature.

5.4.2 XRD measurements

Before and after 7 days in the oven, the material was investigated with XRD to see if the crystal structure had remained the same or changed after the heat treatment. Section 3.4.2 describes the procedure. The data from both measurements were analyzed with TOPAS, peak indexed, and matched with the $I\bar{4}$ space group. The day 0 measurement was to be compared to the measurement of the sample after 7 days in an oven at $220°C$. The results of these two measurements are presented in figure 4.13. It is evident how most of the peaks are shifted slightly and experience broadening in the 7-day measurement. This broadening could be an indication that there is more strain in the crystal lattice after the heat treatment. This strain could be caused by crystal defects such as dislocations, point defects, and precipitates. It is not unreasonable to hypothesize that the temperature hold has led to some of these crystal defects appearing. There is also the possibility that the material has degraded, and new molecules such as di-pentaerythritol have formed, causing more strain in the lattice. Furthermore, the day 7 plot shows that the intensity of the peaks is decreased. A possible explanation for this would be that the crystallinity of the material is decreasing. This can also be confirmed by observing an increased background noise, reminiscent of the results from a slightly more amorphous material.

5.4.3 Raman measurements

The last investigation conducted before and after the seven-day temperature hold experiment was the Raman measurements presented in 3.4.3. This was done so that one would be able to investigate if there were any new bonds detected, or if any bonds had disappeared after the heat treatment. The results from the experiment can be seen in figure 4.14. Here, several of the peaks are marked with red dots. These peaks were found to correspond well with peaks found in other literature [52]. Comparing the day 0 and day 7 plots, it is possible to see a major difference. The day 0 plot shows the characteristic peaks of the material, whilst the day 7 plot seems to have massive amounts of fluorescence, which makes it near impossible to determine what bonds are present. Even though this is the case, it could be worth noting that the wavenumber of the highest intensity of the day 7 plot seems to correspond to the wavenumber of the most intense peak in the day 0 plot. This could

be an indication that even though something has changed, the CH stretched bond still remains. Furthermore, the fact that there is fluorescence on day 7, and not on day 0 is a remarkable thing in and of itself. The presence of fluorescence indicates that there are new excitation states present in the sample that were not present at day 0. These excitation states are lower than those of the material at day 0, which enables the electrons to not just be excited to a virtual state, but rather to a whole new excitation state. When the excited electron eventually falls down to the ground state, it will release a specific energy which is interpreted as fluorescence. Practically this means that on day 7 there are other bonds present than at day 0.

One way one would see fluorescence is if the material has impurities that possess fluorescent properties. However, if this was the case, it would be likely that this was seen already at day 0. Another explanation is that these impurities have reacted with the material creating new fluorescent species. Considering the purity of the material analyzed (98%), and regarding the usually known impurities, the impurity explanation seems not likely. The last and most plausible explanation for the observed fluorescence after seven days is that the material has undergone degradation, leading to the formation of new species with fluorescent properties. One possible organic species with fluorescent properties in Raman would be aromatic compounds. Without knowing more about the species found in the day 7 measurements, it is hard to say exactly what decomposition products are present.

6 Conclusion

The objective of this study was to examine the viability of pentaerythritol as a LHS material in cooking stoves. Basic TES properties of the material such as specific heat capacity, thermal conductivity, and thermal expansion were found. Secondly, specific characteristics of the material related to TES such as the operational temperature range, enthalpy of the heat storage phase change, and useful lifetime of the material were investigated. This second set of investigations was approached from three different angles: depending on the atmospheric conditions, the purity and melting and resolidification of the material, and the time at the maximum operational temperature.

The investigation of the basic TES properties of the material revealed a specific heat capacity increasing from $1.43\,J/gK$ to $2.06\,J/gK$ in the temperature range $40-160°C$. This was found during analysis with DSC, and the result corresponded well with prior studies. The thermal conductivity of the material was found by laserflash to be approximately $1.00\,W/mK$ at $25°C$, and decreased to $0.75\,W/mK$ at $175°C$. At $200°C$, a thermal conductivity of $0.32\,W/mK$ was recorded. This significant drop was caused by the material going through the solid-solid phase change. Thermal conductivity for the material was also found by utilizing the C_p from the DSC measurements and the thermal diffusivity from the laserflash experiment. These values followed the same trend as the laserflash results, but the magnitude of the values was slightly lower, starting at $0.93\,W/mK$ at $25°C$, and decreased to $0.56\,W/mK$ at $175°C$. The thermal expansion investigation involved analyzing the material with XRD upon heating. Here it was concluded that the linear thermal expansion coefficients were $\alpha_a = 1.72 \cdot 10^{-5}$ and $\alpha_c = 15.39 \cdot 10^{-5}$. The larger expansion for α_c could be explained by weaker bonds holding the molecule together on the c-axis.

The atmospheric-dependent investigations with TG and MS indicated that the material degrades faster when oxygen is present. This conclusion was made after observing a lower melting point in synthetic air than in argon ($256.2°C$ vs. $260.0°C$). Furthermore, MS gas detection indicated greater amounts and earlier production of gaseous species in the synthetic air measurements. The main gases found were H_2O and CO_2, but other hydrocarbon gases were also thought to be present. Overall, these observations matched well with previous studies. The second part of the atmospheric-dependent investigation involved testing the material with DSC. Here, the enthalpy of transition for the material was found in synthetic air and argon. The results indicated that the endothermic solid-solid phase change had a higher enthalpy in synthetic air than in argon. A conclusion as to why this was the case has not been made, but speculations such as a more substantial production of gases in synthetic air, and different temperature calibrations have been brought forward to explain the variation in enthalpy. It was also concluded that the atmosphere did not affect the temperatures where the solid-solid phase change took place. The third and final atmosphere-dependent experimental procedure involved thermal cycling of the material in DSC with both a synthetic air and argon atmosphere. It was concluded that the material degrades faster in synthetic air than argon when going through the phase change. After 50 cycles, the maximum degradation in the enthalpy for the endothermic solid-solid phase change was 12.07% in synthetic air from the initial measurement, and 1.35% in an argon atmosphere. Furthermore, the decrease in the starting temperature was more significant for the synthetic air measurements. These observations match the results seen in the TG/MS experiment.

The resolidification- and purity-dependent investigations were brought forward to find out if and how much the TES properties of the material are affected by purity, and melting and solidifying the material. Therefore, three different material purities from two sample providers (4 samples

in total), and a fifth sample made up of melted and resolidified material were analyzed. DSC investigations concluded that the higher the purity, the higher the enthalpy of the endothermic solid-solid phase change. Furthermore, melting and resolidifying the material leads to a significant decrease in enthalpy. It was also seen that the enthalpy values varied when looking at the different material providers. Regarding the temperatures associated with the endothermic phase change, it was concluded that the higher the material purity and unmelted material, one have a higher starting temperature. In total, a larger amount of impurities means that the material will have an endothermic solid-solid phase change at lower temperatures with a smaller enthalpy of change. The thermal cycling investigations made with DSC depending on the purity and melted and resolidified material did not find any conclusive evidence to say if the material degrades faster when resolidified or at lower purity. Raman spectroscopy investigations of unmelted and resolidified material proved that the same bonds are found before and after melting/resolidifying the material. There was a slight increase in the background which could prove that some new species with fluorescence had been created during melting.

The temperature hold investigations studied if and how the TES properties of the material would be affected by time at the maximum operational temperature. The program involved holding the material at $220°C$ for seven days. Here, it was concluded that there was a significant degradation of the material happening which lead to a decrease in enthalpy from $273.78\ J/g$ to $171.45\ J/g$ from day 0 to day 7. Furthermore, this material degradation leads to a significant decrease in the starting temperature of the endothermic solid-solid phase transition. The second investigation of the material from the temperature hold experiment was made with XRD. Here, the goal was to find out if the crystal structure changes after the temperature hold. From the results, one could see a peak shift, peak broadening, and a peak reduction after 7 days. Reasons for this could be more lattice strain caused by crystal defects, and a lower crystallinity. Lastly, Raman analysis was also done on the day 0 and day 7 material. After 7 days, there was a great amount of fluorescence which could be caused by fluorescent species such as aromatic compounds. Even though no peaks on day 7 could be distinguished, the maximum intensities on day 0 and day 7 were at the same wavenumbers indicating that there are still bonds remaining.

To be able to conclude if the material is suitable for LHS in a cooking stove, the deciding factor is the degradation of the material when in use. It is clear that the best results were obtained with high material purity, an inert operating atmosphere, and the lowest possible maximum operating temperature above the solid-solid phase change. With more investigations of the material in these operating conditions, one could reveal if LHS with pentaerythritol is a possibility. In conclusion, the use of pentaerythritol for thermal energy storage in a domestic cooking stove seems plausible, however, the specific operating conditions, particularly atmosphere, and maximum temperature are critical to the longevity and efficiency of the material.

7 Further work

The presented study has provided valuable insight into the viability of pentaerythritol as a latent heat storage material. Despite the findings of the substantial degradation upon heating, there are still aspects of storing heat within the candidate material that should be explored.

Firstly, there could be made changes to how the melted material samples were made. Instead of melting and resolidifying material in an uncontrolled atmosphere, it would be possible to do this in an inert atmosphere. This could potentially reduce the degradation of the material upon melting, as it seems that it degrades slower when there is a lack of oxygen present. Furthermore, it would be of interest to investigate if the results from the temperature hold experiment would be different if the procedure took place in an inert atmosphere. One could also investigate how a lower maximum operational temperature affects the degradation in the temperature hold experiment.

In this study, there is a lack of information when it comes to the mesophase of the material. It would be of value to carry out XRD and Raman studies of the material over the entire temperature range, including the melting point. This could potentially form a broader picture of precisely how the material degrades, and what alternative species are formed. A nuclear magnetic resonance (NMR) analysis of the material, could also offer more insight into this. The species formed upon heating could be contributing to the material properties. Furthermore, it would be interesting to investigate how varying amounts of specific impurities affect the LHS capabilities of the material. Are different species created with different types of impurities, and how does this affect the LHS properties?

As presented in this study, the material was thermally cycled 50 times with the intent to reveal the degradation of the LHS properties. The number of cycles is nowhere near the amount the material would be required to withstand in an operative scenario. Conducting an accelerated lifetime study where one investigates how the material degrades further could be insightful. This accelerated lifetime study would consist of a much greater number of thermal cycles and should be conducted in an inert atmosphere, as this is where the material seems to have the greatest potential as a LHS material. Here, also investigating the exothermic phase transition would give valuable information into the heat discharge of the material.

Lastly, there have already been made investigations into how one could improve the LHS properties of pentaerythritol. Enhancing the material by creating composites could prove to solve problems like low thermal diffusivity, or high-temperature degradation.

Bibliography

[1] Magnus Bengt Inge Ramberg. 'Thermal Energy Storage Materials to Improve Quality of Life in Developing Countries'. In: *TMT4500 Materials Technology, Specialization Project, NTNU* (2022).

[2] WHO. *Household air pollution*. 2022. URL: https://www.who.int/news-room/fact-sheets/detail/household-air-pollution-and-health (visited on 01/06/2023).

[3] Francis Agyenim, Philip Eames and Mervyn Smyth. 'A comparison of heat transfer enhancement in a medium temperature thermal energy storage heat exchanger using fins'. In: *Solar Energy* 83.9 (2009), pp. 1509–1520. DOI: 10.1016/j.solener.2009.04.007.

[4] Pushpendra Kumar Singh Rathore and Shailendra Kumar Shukla. 'Potential of macroencapsulated PCM for thermal energy storage in buildings: A comprehensive review'. In: *Construction and Building Materials* 225 (2019), pp. 723–744. DOI: 10.1016/j.conbuildmat.2019.07.221.

[5] Kinga Pielichowska and Krzysztof Pielichowski. 'Phase change materials for thermal energy storage'. In: *Progress in Materials Science* 65 (2014), pp. 67–123. DOI: 10.1016/j.pmatsci.2014.03.005.

[6] Yolanda A. Criado, Mónica Alonso and J. Carlos Abanades. 'Kinetics of the CaO/Ca(OH)2 Hydration / Dehydration Reaction for Thermochemical Energy Storage Applications'. In: *Industrial & Engineering Chemistry Research* 53.32 (2014), pp. 12594–12601. DOI: 10.1021/ie404246p.

[7] Ahmad Mojiri, Nikola Grbac, Brendan Bourke and Gary Rosengarten. 'D-mannitol for medium temperature thermal energy storage'. In: *Solar Energy Materials and Solar Cells* 176 (2018), pp. 150–156. DOI: 10.1016/j.solmat.2017.11.028.

[8] Tao Xu, Qinglin Chen, Gongsheng Huang, Zhengguo Zhang, Xuenong Gao and Shushen Lu. 'Preparation and thermal energy storage properties of d-Mannitol/expanded graphite composite phase change material'. In: *Solar Energy Materials and Solar Cells* 155 (2016), pp. 141–146. DOI: 10.1016/j.solmat.2016.06.003.

[9] Sigma-Aldrich. *D-Mannitol, SA*. 2023. URL: https://www.sigmaaldrich.com/NO/en/product/sial/m4125 (visited on 11/06/2023).

[10] Guruprasad Alva, Lingkun Liu, Xiang Huang and Guiyin Fang. 'Thermal energy storage materials and systems for solar energy applications'. In: *Renewable and Sustainable Energy Reviews* 68 (2017), pp. 693–706. DOI: 10.1016/j.rser.2016.10.021.

[11] Nan Sheng, Kaixin Dong, Chunyu Zhu, Tomohiro Akiyama and Takahiro Nomura. 'Thermal conductivity enhancement of erythritol phase change material with percolated aluminum filler'. In: *Materials Chemistry and Physics* 229 (2019), pp. 87–91. DOI: 10.1016/j.matchemphys.2019.02.033.

[12] Thermo Scientific. *meso-Erythritol, 99%, TS*. 2023. URL: https://www.fishersci.com/shop/products/meso-erythritol-99-thermo-scientific-2/AC117825000#?keyword=Erythritol (visited on 11/06/2023).

[13] Saman Nimali Gunasekara, Monika Ignatowicz, Justin NingWei Chiu and Viktoria Martin. 'Thermal conductivity measurement of erythritol, xylitol, and their blends for phase change material design: A methodological study'. In: *International Journal of Energy Research* 43.5 (2019), pp. 1785–1801. DOI: https://doi.org/10.1002/er.4403.

[14] Sigma-Aldrich. *Xylitol, SA*. 2023. URL: https://www.sigmaaldrich.com/NO/en/product/aldrich/w507930 (visited on 11/06/2023).

[15] Mohammed M Farid, Amar M Khudhair, Siddique Ali K Razack and Said Al-Hallaj. 'A review on phase change energy storage: materials and applications'. In: *Energy Conversion and Management* 45.9 (2004), pp. 1597–1615. DOI: 10.1016/j.enconman.2003.09.015.

[16] Sigma-Aldrich. *Paraffin wax, SA*. 2023. URL: https://www.sigmaaldrich.com/NO/en/product/aldrich/411663 (visited on 11/06/2023).

[17] Zhanxiu Chen and Guanyi Chen. 'Experimental Study on the Thermal Storage Performance and Preparation of Glycerin Mixtures Used in the Phase Change Wall'. In: *2010 WASE International Conference on Information Engineering*. Vol. 2. 2010, pp. 51–54. DOI: 10.1109/ICIE.2010.108.

[18] Sigma-Aldrich. *Glycerol, SA*. 2023. URL: https://www.sigmaaldrich.com/NO/en/product/aldrich/w252506 (visited on 11/06/2023).

[19] K. P. Venkitaraj and S. Suresh. 'Experimental thermal degradation analysis of pentaerythritol with alumina nano additives for thermal energy storage application'. In: *Journal of Energy Storage* 22 (2019), pp. 8–16. DOI: 10.1016/j.est.2019.01.017.

[20] K. P. Venkitaraj and S. Suresh. 'Experimental study on thermal and chemical stability of pentaerythritol blended with low melting alloy as possible PCM for latent heat storage'. In: *Experimental Thermal and Fluid Science* 88 (2017), pp. 73–87. DOI: 10.1016/j.expthermflusci.2017.05.018.

[21] Sigma-Aldrich. *Pentaerythritol for synthesis, SA*. 2023. URL: http://www.sigmaaldrich.com/ (visited on 11/06/2023).

[22] Biao Feng, Jing Tu, Ju-Wei Sun, Li-Wu Fan and Yi Zeng. 'A molecular dynamics study of the effects of crystalline structure transition on the thermal conductivity of pentaerythritol as a solid-solid phase change material'. In: *International Journal of Heat and Mass Transfer* 141 (2019), pp. 789–798. DOI: 10.1016/j.ijheatmasstransfer.2019.07.017.

[23] Dineshkumar Mani, M. K. Saranprabhu and K. S. Rajan. 'Intensification of thermal energy storage using copper-pentaerythritol nanocomposites for renewable energy utilization'. In: *Renewable Energy* 163 (2021), pp. 625–634. DOI: 10.1016/j.renene.2020.08.119.

[24] Zhaofeng Dai, Yuanzhi Gao, Changling Wang, Dongxu Wu, Zhu Jiang, Xiaohui She, Yulong Ding, Xiaosong Zhang and Dongliang Zhao. 'Oriented High Thermal Conductivity Solid–Solid Phase Change Materials for Mid-Temperature Solar-Thermal Energy Storage'. In: *ACS Applied Materials & Interfaces* 15.22 (2023), pp. 26863–26871. DOI: 10.1021/acsami.3c04429.

[25] Sergio Santos-Moreno, Stefania Doppiu, Gabriel A. Lopez, Nevena Marinova, Ángel Serrano, Elena Silveira and Elena Palomo del Barrio. 'Study of the Phase Transitions in the Binary System NPG-TRIS for Thermal Energy Storage Applications'. In: *Materials* 13.5 (2020), p. 1162. DOI: 10.3390/ma13051162.

[26] Sigma-Aldrich. *Tris(hydroxymethyl)aminomethane, SA*. 2023. URL: https://www.sigmaaldrich.com/NO/en/product/mm/108382 (visited on 11/06/2023).

[27] Sigma-Aldrich. *1,1,1-Tris(hydroxymethyl)ethane, SA*. 2023. URL: https://www.sigmaaldrich.com/NO/en/product/aldrich/t87807 (visited on 11/06/2023).

[28] Nan Zhang, Yanlin Song, Yanxia Du, Yanping Yuan, Guangming Xiao and Yewei Gui. 'A Novel Solid–Solid Phase Change Material: Pentaglycerine/Expanded Graphite Composite PCMs'. In: *Advanced Engineering Materials* 20.10 (2018), p. 1800237. DOI: https://doi.org/10.1002/adem.201800237.

[29] Sigma-Aldrich. *2,2-Dimethyl-1,3-propanediol 99, SA*. 2023. URL: https://www.sigmaaldrich.com/NO/en/product/aldrich/538256 (visited on 11/06/2023).

[30] Dhanesh Chandra, Raja Chellappa and Wen-Ming Chien. 'Thermodynamic assessment of binary solid-state thermal storage materials'. In: *Journal of Physics and Chemistry of Solids*. Proceedings of the 11th International Conference on High Temperature Materials Chemistry (HTMC-XI) 66.2 (2005), pp. 235–240. DOI: 10.1016/j.jpcs.2004.08.047.

[31] B. Praveen and S. Suresh. 'Experimental study on heat transfer performance of neopentyl glycol/CuO composite solid-solid PCM in TES based heat sink'. In: *Engineering Science and Technology, an International Journal* 21.5 (2018), pp. 1086–1094. DOI: 10.1016/j.jestch.2018.07.010.

[32] B. Eanest Jebasingh and A. Valan Arasu. 'A detailed review on heat transfer rate, supercooling, thermal stability and reliability of nanoparticle dispersed organic phase change material for low-temperature applications'. In: *Materials Today Energy* 16 (2020), p. 100408. DOI: 10.1016/j.mtener.2020.100408.

[33] J.S. Wettlaufer and M. Grae Worster. 'Premelting Dynamics'. In: *Annual Review of Fluid Mechanics* 38.1 (2006), pp. 427–452. DOI: 10.1146/annurev.fluid.37.061903.175758.

[34] Ahmet Sarı and Ali Karaipekli. 'Thermal conductivity and latent heat thermal energy storage characteristics of paraffin/expanded graphite composite as phase change material'. In: *Applied Thermal Engineering* 27.8 (2007), pp. 1271–1277. DOI: 10.1016/j.applthermaleng.2006.11.004.

[35] A. Hussein, M. S. Abd-Elhady, M. N. El-Sheikh and H. T. El-Metwally. 'Improving Heat Transfer Through Paraffin Wax, by Using Fins and Metallic Strips'. In: *Arabian Journal for Science and Engineering* 43.9 (2018), pp. 4433–4441. DOI: 10.1007/s13369-017-2923-2.

[36] Jun Harada, Takafumi Shimojo, Hideaki Oyamaguchi, Hiroyuki Hasegawa, Yukihiro Takahashi, Koichiro Satomi, Yasutaka Suzuki, Jun Kawamata and Tamotsu Inabe. 'Directionally tunable and mechanically deformable ferroelectric crystals from rotating polar globular ionic molecules'. In: *Nature Chemistry* 8.10 (2016), pp. 946–952. DOI: 10.1038/nchem.2567.

[37] J. Timmermans. 'Plastic crystals: A historical review'. In: *Journal of Physics and Chemistry of Solids* 18.1 (1961), pp. 1–8. DOI: 10.1016/0022-3697(61)90076-2.

[38] M. Barrio, J. Font, J. Muntasell, J. Navarro and J. Ll. Tamarit. 'Applicability for heat storage of binary systems of neopentylglycol, pentaglycerine and pentaerythritol: A comparative analysis'. In: *Solar Energy Materials* 18.1 (1988), pp. 109–115. DOI: 10.1016/0165-1633(88)90051-2.

[39] R. Sakamoto, M. Kamimoto, Y. Takahashi, Y. Abe, K. Kanari and T. Ozawa. 'Investigation of latent heat-thermal energy storage materials. III. Thermoanalytical evaluation of pentaerythritol'. In: *Thermochimica Acta* 77.1 (1984), pp. 241–249. DOI: 10.1016/0040-6031(84)87063-X.

[40] Zbigniew A. Dreger, Yogendra M. Gupta, Choong-Shik Yoo and Hyunchae Cynn. 'High-Pressure-Induced Phase Transitions in Pentaerythritol: X-ray and Raman Studies'. In: *The Journal of Physical Chemistry B* 109.47 (2005), pp. 22581–22587. DOI: 10.1021/jp0582181.

[41] Venkitaraj K.p and S Suresh. 'Experimental study on the thermal storage performance and non-isothermal crystallization kinetics of pentaerythritol blended with low melting metal'. In: *Thermochimica Acta* 662 (2018), pp. 75–89. DOI: 10.1016/j.tca.2018.02.007.

[42] Yoshio Takahashi, Masayuki Kamimoto, Yoshiyuki Abe, Yuji Nagasaka and Akira Nagashima. 'Heat Capacity, Heat of Transition, and Thermal Conductivity of Pentaerythritol and Its Slurry'. In: *Netsu Bussei* 2.1 (1988), pp. 53–58. DOI: 10.2963/jjtp.2.53.

[43] W. Wagner and A. Pruß. 'The IAPWS Formulation 1995 for the Thermodynamic Properties of Ordinary Water Substance for General and Scientific Use'. In: *Journal of Physical and Chemical Reference Data* 31.2 (2002), pp. 387–535. DOI: 10.1063/1.1461829.

[44] E. Murrill and L. Breed. 'Solid—solid phase transitions determined by differential scanning calorimetry: Part I. Tetrahedral substances'. In: *Thermochimica Acta* 1.3 (1970), pp. 239–246. DOI: 10.1016/0040-6031(70)80027-2.

[45] Isamu Nitta, Tokunosuké Watanabé, Syûzô Seki and Masanobu Momotani. 'On the Phase Transition in Pentaerythritol (III)'. In: *Proceedings of the Japan Academy* 26.10 (1950), pp. 19–24. DOI: 10.2183/pjab1945.26.10_19.

[46] Dhanesh Chandra, Joan J. Fitzpatrick and Gary Jorgensen. 'The Structure and Lattice Parameters of Pentaerythritol Above and Below its Phase-Transition Temperature'. In: *Advances in X-Ray Analysis* 28 (1984), pp. 353–360. DOI: 10.1154/S0376030800014191.

[47] Terrence J. Simons, Rohan L. de Silva and Dennis E. Creasy. 'Crystallisation of pentaerythritol. III. Impurity distribution coefficients'. In: *Journal of Chemical Technology and Biotechnology* 32.4 (1982), pp. 518–524. DOI: 10.1002/jctb.5030320404.

[48] Feng Zhang, Jun Zhang and Daoxing Sun. 'Study on Thermal Decomposition of Intumescent Fire-Retardant Polypropylene by TG/Fourier Transform Infrared'. In: *Journal of Thermoplastic Composite Materials* 22.6 (2009), pp. 681–701. DOI: 10.1177/0892705709093502.

[49] Pin Lv, Zhengzhou Wang, Keliang Hu and Weicheng Fan. 'Flammability and thermal degradation of flame retarded polypropylene composites containing melamine phosphate and pentaerythritol derivatives'. In: *Polymer Degradation and Stability* 90.3 (2005), pp. 523–534. DOI: 10.1016/j.polymdegradstab.2005.04.003.

[50] Sergii Guzii, T Kurska, Yurii Otrosh, P Balduk and Y Ivanov. 'Features of the organic-mineral intumescent paints structure formation for wooden constructions fire protection'. In: *IOP Conference Series: Materials Science and Engineering* 1162 (2021), p. 012003. DOI: 10.1088/1757-899X/1162/1/012003.

[51] J. Park, Rongshun Zhu and M. Lin. 'Thermal decomposition of ethanol. I. Ab Initio molecular orbital/Rice–Ramsperger–Kassel–Marcus prediction of rate constant and product branching ratios'. In: *The Journal of Chemical Physics* 117 (2002), pp. 3224–3231. DOI: 10.1063/1.1490601.

[52] Ta-Ryeong Park, Zbigniew A. Dreger and Yogendra M. Gupta. 'Raman Spectroscopy of Pentaerythritol Single Crystals under High Pressures'. In: *The Journal of Physical Chemistry B* 108.10 (2004), pp. 3174–3184. DOI: 10.1021/jp031179d.

[53] J.W. Arblaster. 'Crystallographic Properties of Platinum'. In: *Platinum Metals Review (UK)* 41.1 (1997), pp. 12–21. URL: https://technology.matthey.com/journal (visited on 26/05/2023).

[54] Afshin J. Ghajar and Yunus A. Cengel Dr. *Heat and Mass Transfer: Fundamentals and Applications*. 5th. McGraw-Hill Education, 2014.

[55] Kim Song and Donald Le. *Bond Energies*. 2013. URL: https://chem.libretexts.org/Bookshelves/Physical_and_Theoretical_Chemistry_Textbook_Maps/Supplemental_Modules_(Physical_and_Theoretical_Chemistry)/Chemical_Bonding/Fundamentals_of_Chemical_Bonding/Bond_Energies (visited on 15/06/2023).

A Appendix

Table A.1: Average bond energies for relevant atomic bonds in the material pentaerythritol. Values found on Libretext Chemistry [55]

Bond	**Bond energy (kJ/mol)**
C-C	347
C-O	358
C-H	413
O-H	467

Table A.2: Fractional parts of the initial weights of pentaerythritol samples during thermal cycling. Each sample was weighed manually every 10 cycles.

	SA99		**SA98**		**P98**		**P86**		**MP98**	
Cycle	**Air**	**Argon**	**Air**	**Argon**	**Air**	**Argon**	**Air**	**Argon**	**Air**	**Argon**
0	1	1	1	1	1	1	1	1	1	1
10	0.95	0.94	0.94	0.93	0.93	0.94	0.94	0.95	0.95	0.94
20	0.90	0.88	0.89	0.87	0.89	0.87	0.90	0.90	0.91	0.88
30	0.85	0.82	0.84	0.82	0.80	0.82	0.84	0.86	0.86	0.83
40	0.79	0.76	0.78	0.75	0.73	0.77	0.77	0.82	0.82	0.77
50	0.73	0.70	0.72	0.70	0.65	0.69	0.68	0.78	0.77	0.72

Table A.3: Values of thermal diffusivity, thermal conductivity and specific heat capacity from the laserflash measurements. Specific heat capacity also included from the DSC, and a new calculated thermal conductivity was calculated using equation 2.2. A density of $1.205 g/cm^3$ was used.

Temp	α**(mm²/s)**	**k(W/mK)**	**C_p(J/gK)**	**C_p(J/gK) - DSC**	**k(W/mK) - DSC**
25	0.521	1.000	1.722	1.480	0.929
100	0.342	0.853	2.072	1.704	0.702
150	0.254	0.783	2.557	1.982	0.607
175	0.211	0.746	2.939	2.205	0.561
200	0.088	0.324	3.068	-	-

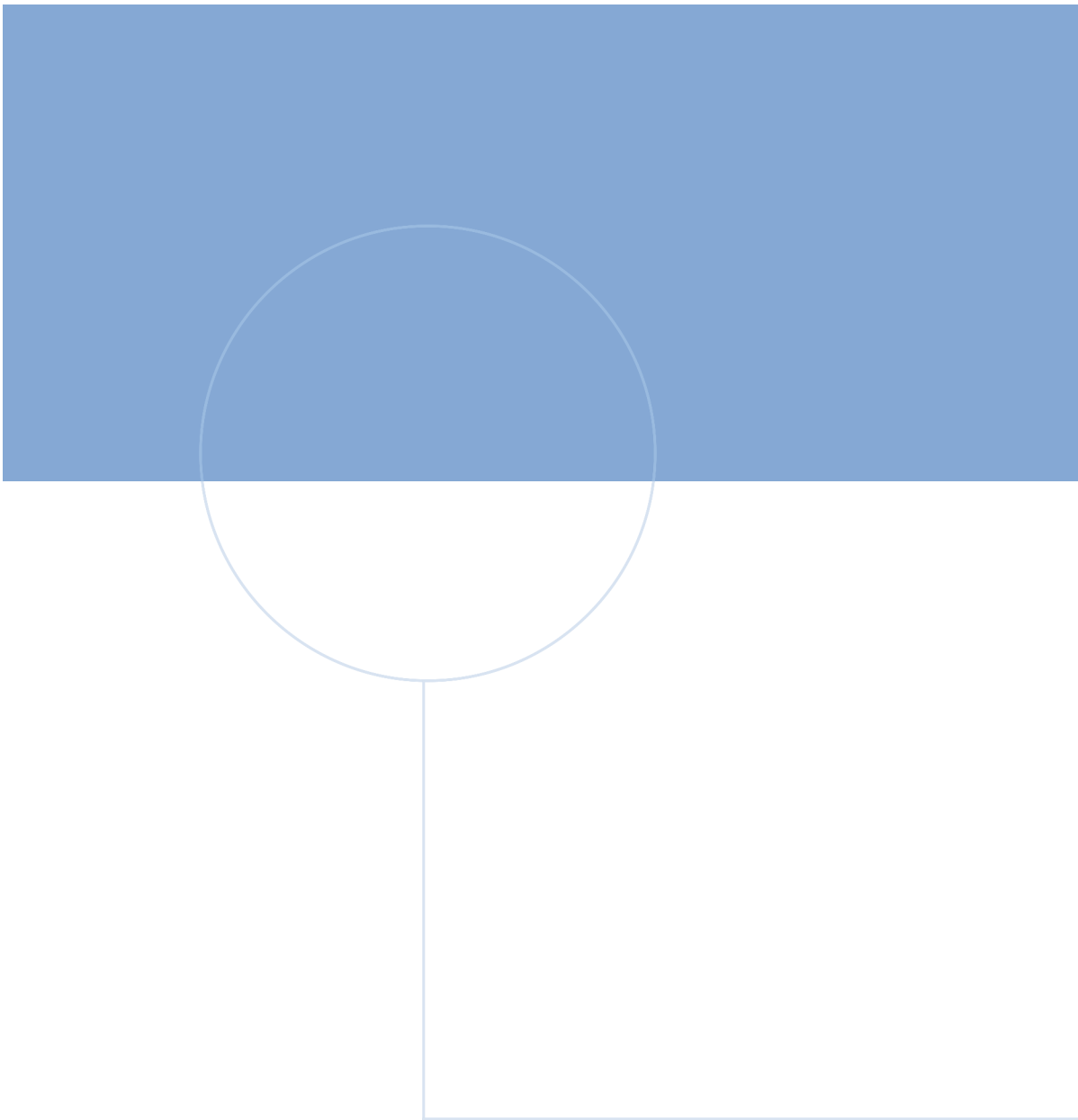

NTNU

Norwegian University of
Science and Technology